Article

Cell

A Site of Vulnerability on the Influenza Virus Hemagglutinin Head Domain Trimer Interface

Graphical Abstract

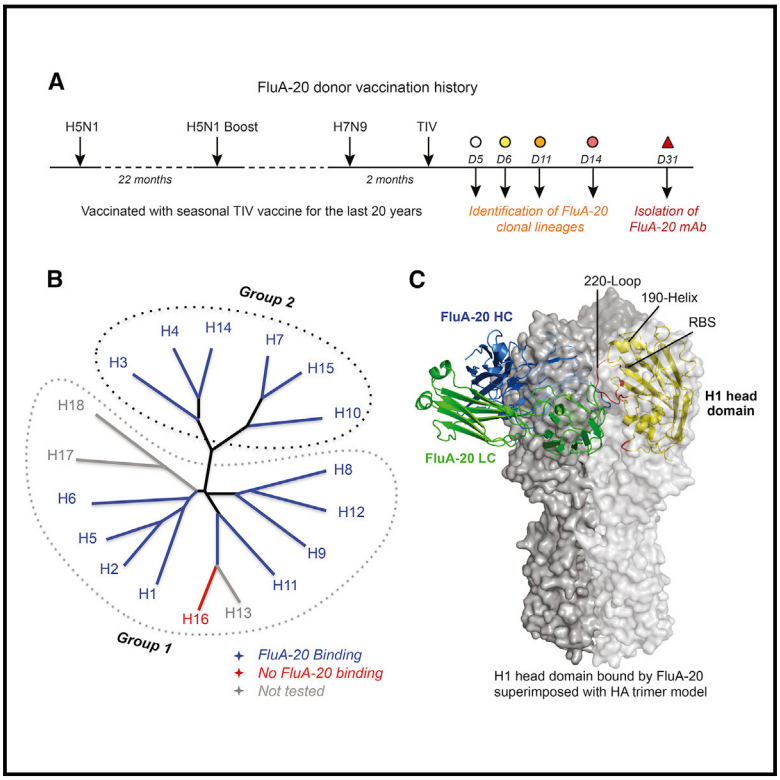

Highlights

- FluA-20 isolated from a healthy donor with extensive influenza vaccination history
- FluA-20 protects against all major influenza A subtypes that infect humans
- FluA-20 recognizes a unique conserved site in the trimer interface of the HA head
- FluA-20 binds to the uncleaved form of HA trimer and disrupts trimer integrity

Authors

Sandhya Bangaru, Shanshan Lang, Michael Schotsaert, ..., Andrew B. Ward, Ian A. Wilson, James E. Crowe, Jr.

Correspondence

wilson@scripps.edu (I.A.W.), james.crowe@vanderbilt.edu (J.E.C.)

In Brief

Antibodies targeting a novel site in the head domain of hemagglutinin afford broad protection against influenza.

Bangaru et al., 2019, Cell *177*, 1136–1152
May 16, 2019
https://doi.org/10.1016/j.cell.2019.04.011

CellPress

Cell

Article

A Site of Vulnerability on the Influenza Virus Hemagglutinin Head Domain Trimer Interface

Sandhya Bangaru,[1,11] Shanshan Lang,[2,11] Michael Schotsaert,[3,6] Hillary A. Vanderven,[4] Xueyong Zhu,[2] Nurgun Kose,[5] Robin Bombardi,[5] Jessica A. Finn,[1] Stephen J. Kent,[4] Pavlo Gilchuk,[5] Iuliia Gilchuk,[5] Hannah L. Turner,[2] Adolfo García-Sastre,[3,6,7] Sheng Li,[8] Andrew B. Ward,[2] Ian A. Wilson,[2,9,12,*] and James E. Crowe, Jr.[1,5,10,12,13,*]

[1]Department of Pathology, Microbiology and Immunology, Vanderbilt University Medical Center, Nashville, TN 37232, USA
[2]Department of Integrative Structural and Computational Biology, The Scripps Research Institute, La Jolla, CA 92037, USA
[3]Department of Microbiology, Icahn School of Medicine at Mount Sinai, New York, NY 10029, USA
[4]Department of Microbiology and Immunology, Peter Doherty Institute for Infection and Immunity, University of Melbourne, Melbourne, Victoria, Australia
[5]The Vanderbilt Vaccine Center, Vanderbilt University Medical Center, Nashville, TN 37232, USA
[6]Global Health and Emerging Pathogens Institute, Icahn School of Medicine at Mount Sinai, New York, NY 10029, USA
[7]Department of Medicine, Icahn School of Medicine at Mount Sinai, New York, NY 10029, USA
[8]Department of Medicine and Biomedical Sciences, School of Medicine, University of California, San Diego, CA 92093, USA
[9]The Skaggs Institute for Chemical Biology, The Scripps Research Institute, La Jolla, CA 92037, USA
[10]Department of Pediatrics, Vanderbilt University Medical Center, Nashville, TN 37232, USA
[11]These authors contributed equally
[12]Senior author
[13]Lead Contact
*Correspondence: wilson@scripps.edu (I.A.W.), james.crowe@vanderbilt.edu (J.E.C.)
https://doi.org/10.1016/j.cell.2019.04.011

SUMMARY

Here, we describe the discovery of a naturally occurring human antibody (Ab), FluA-20, that recognizes a new site of vulnerability on the hemagglutinin (HA) head domain and reacts with most influenza A viruses. Structural characterization of FluA-20 with H1 and H3 head domains revealed a novel epitope in the HA trimer interface, suggesting previously unrecognized dynamic features of the trimeric HA protein. The critical HA residues recognized by FluA-20 remain conserved across most subtypes of influenza A viruses, which explains the Ab's extraordinary breadth. The Ab rapidly disrupted the integrity of HA protein trimers, inhibited cell-to-cell spread of virus in culture, and protected mice against challenge with viruses of H1N1, H3N2, H5N1, or H7N9 subtypes when used as prophylaxis or therapy. The FluA-20 Ab has uncovered an exceedingly conserved protective determinant in the influenza HA head domain trimer interface that is an unexpected new target for anti-influenza therapeutics and vaccines.

INTRODUCTION

Currently, influenza A virus (IAV) strains from subtypes H1N1 and H3N2, as well as influenza B viruses, are in human circulation and cause seasonal epidemics. Poor matches of the predicted vaccine strains with drifted seasonal viruses can lead to severe influenza seasons (Bridges et al., 2000; Carrat and Flahault, 2007; Nordin et al., 2001). Additionally, other zoonotic IAVs with H1, H3, H5, H6, H7, H9, and H10 hemagglutinins (HAs) have caused sporadic outbreaks of human infections, some with exceedingly high morbidity and mortality rates (Freidl et al., 2014; Neumann and Kawaoka, 2015). New influenza viruses emerging from genomic reassortment with drastically altered antigenicity can cause global pandemics.

The HA of influenza is one of the two main glycoproteins on the viral surface and a major target of neutralizing antibodies (Abs). Based on structure and antigenicity, there are eighteen defined subtypes (H1–H18) of IAV HAs belonging to two broad groups (Nobusawa et al., 1991; Russell et al., 2004; Tong et al., 2013). Influenza HA consists of an antigenically variable globular head domain containing the receptor-binding site (RBS) for viral attachment and a more conserved stem domain that mediates fusion of viral and cell membranes in the endosome (Carr and Kim, 1993; Weis et al., 1988; Wilson et al., 1981). The HA head domain is the immunodominant domain of the protein and is the target of most Ab responses induced by IAV vaccines or infection (Altman et al., 2015; Angeletti et al., 2017; Caton et al., 1982; Das et al., 2013; Gerhard et al., 1981). However, most head-domain-specific Abs exhibit a narrow breadth of protection due to the high level of sequence and antigenic diversity and the incorporation of large numbers of glycans in this domain to evade immune recognition.

Two classes of broadly neutralizing Abs (bnAbs) against influenza HA have been discovered (Julien et al., 2012; Laursen and Wilson, 2013). The stem-targeted bnAbs, such as the murine monoclonal Ab (mAb) C179 and human mAbs CR6261, F10, and A6, have broad and heterosubtypic activities, some of which can target nearly all strains of HA across various subtypes and subgroups, e.g., CR9114 and MEDI8852 (Corti et al., 2010, 2011; Dreyfus et al., 2013, 2012; Ekiert et al., 2009, 2011; Friesen et al., 2014; Joyce et al., 2016; Kallewaard et al., 2016; Kashyap

A

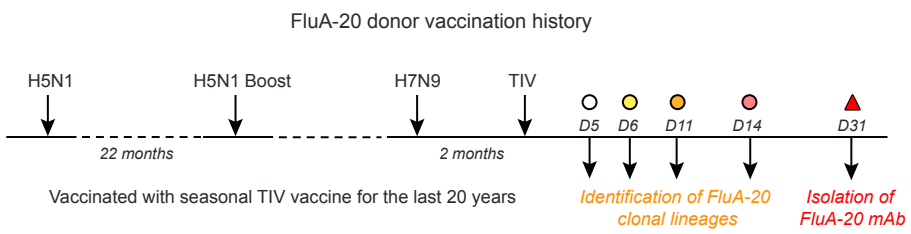

B

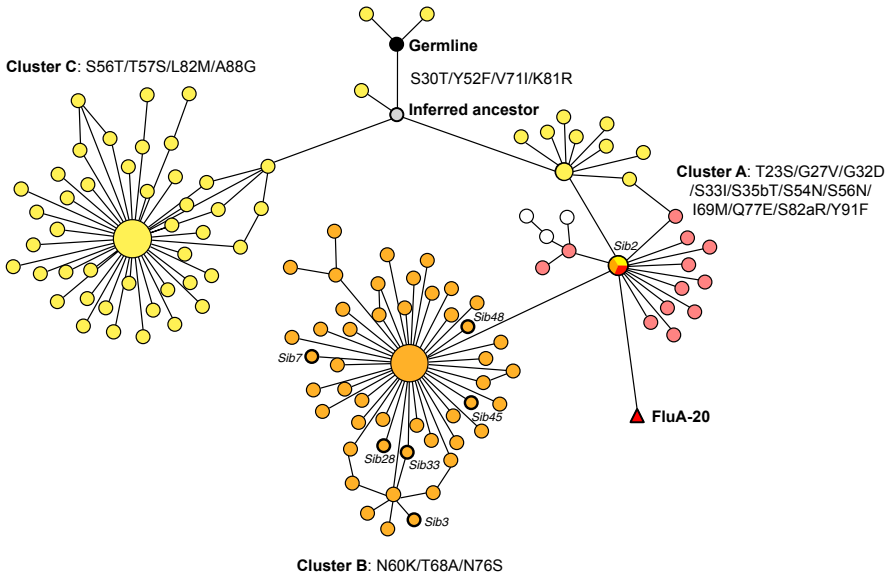

C

		Group 1														Group 2										
Subtype		H1				H2	H5		H6	H8	H9		H11	H12	H16	H3			H4	H7			H10	H14	H15	
HA from indicated strain		A/Fort Monmouth/1/1947	A/Texas/36/1991	A/Solomon Islands/03/2006	A/California/04/2009	A/Singapore/1/1957	A/Vietnam/1203/2004	A/Indonesia/05/2005	A/Taiwan/2/2013	A/turkey/Ontario/6118/1967	A/turkey/Wisconsin/1/1966	A/Hong Kong/1073/1999	A/duck/Memphis/546/1974	A/duck/Alberta/60/1976	A/black-headedgull/Sweden/4/1999	A/Hong Kong/1/1968	A/California/07/2004	A/Texas/50/2012	A/duck/Czechoslovakia/1956	A/New York/107/2003	A/Shanghai/2/3013	A/Netherlands/219/2003	A/chicken/Germany/N/1949	A/mallard duck/Astrakhan/263/1982	A/shearwater/WesternAustralia/25 76/1979	
EC50 (ng/mL)	FluA-20	7	9	8	10	9	142	16	61	5	22	7	72	6	>	8	8	6	7	>	12	6	37	7	7	
	rFluA-20	7	8	8	12	11	133	16	63	5	16	7	76	6	>	9	9	7	7	>	13	5	41	7	7	
	UCA	17	15	10	51	28	>	>	342	>	>	52	>	>	>	21	>	>	13	>	>	33	>	>	>	
	CR6261	43	25	13	12	>	31	26	46	>	>	>	>	>	245	>	>	>	23	>	>	>	>	>	61	

Figure 1. Network Analysis of Sequences Clonally Related to FluA-20 and FluA-20 Reactivity to Diverse HAs

(A) Timeline showing the vaccination history of FluA-20 donor and the time points from which FluA-20 (triangle) and its clonally related siblings (circles) were identified.

(B) Nodes represent unique sequences observed, with the size of the node correlating to the count of replicate sequences observed. The color of each node denotes the time point at which it was found: white, day 5; yellow, day 6; orange, day 11; and pink, day 14. The black node represents the V_H4-61/J_H4 germline sequence, and the gray node represents an inferred common ancestor. The maroon, triangle-shaped node represents FluA-20. Edges drawn between nodes show that those sequences are more closely related to each other than to any other sequence. Edge distances are arbitrary and used only to visually clarify the graph. The somatic variants of FluA-20 that were expressed and tested are indicted.

(legend continued on next page)

et al., 2008, 2010; Lang et al., 2017; Okuno et al., 1993; Smirnov et al., 1999). These bnAbs recognize the highly conserved stem region and block the viral fusion machinery. Stem Abs often interact with FcγR on effector cells to mediate Ab-dependent cellular cytotoxicity (ADCC) and protection *in vivo* (Corti et al., 2011; DiLillo et al., 2016, 2014; He et al., 2015).

A second class of bnAbs targeting the HA head domain also has been discovered (Ekiert et al., 2012; Hong et al., 2013; Joyce et al., 2016; Lee et al., 2014, 2012; Thornburg et al., 2016; Whittle et al., 2011; Xu et al., 2013; Yoshida et al., 2009; Zhu et al., 2013). Most of these head-targeted bnAbs recognize the RBS and block viral attachment and entry. Most head-targeted bnAbs have restricted patterns of recognition within a subtype—for example, the H1-specific 5J8 and CH65 and H2-specific 8M2 Abs (Laursen and Wilson, 2013; Lee et al., 2014; Schmidt et al., 2015; Thornburg et al., 2016; Whittle et al., 2011; Xu et al., 2013). A few exceptions are C05, F045-92, and S139/1, which react with the HA head domain from more than one HA subtype (Ekiert et al., 2012; Lee et al., 2014, 2012; Yoshida et al., 2009). However, their heterosubtypic activities are not extensive, and they heavily rely on the avidity of bivalent immunoglobulin G (IgG) molecules to attain potent binding (~nM K_D) and increased breadth.

Here, we report a broadly protective, naturally occurring human Ab, designated FluA-20, that targets IAVs with exceptional breadth and affinity. The Ab recognizes the HA head domain from nearly all subtypes of influenza A viruses, with K_D values extending to low nanomolar, even in monomeric antigen-binding fragment (Fab) form. The mAb protects mice from sub-lethal and lethal challenges of various pathogenic IAV strains for humans (H1N1, H5N1, H3N2, and H7N9). Structural studies of FluA-20 with the HA head domain revealed a novel epitope on the non-RBS side of the 220-loop and the adjacent 90-loop. The key residues recognized by FluA-20 remain extremely well conserved across diverse subtypes. The epitope is largely buried in the peripheral interface of the native HA trimer. The findings suggest that the HA trimer interface (TI) can be exposed, perhaps transiently or partially. Although the Ab recognizes the head domain, it does not mediate conventional neutralizing activity *in vitro*, but rather, it exhibits a new phenotype of activity comprising the capacity to disrupt HA trimers and inhibit cell-to-cell spread of virus.

RESULTS

Isolation of Broadly Reactive Human mAb FluA-20

The donor had received annual licensed inactivated seasonal vaccines for over two decades and also had participated previously in clinical trials of experimental H5N1 and H7N9 subunit vaccines (Figure 1A). The first H5 vaccine was a monovalent inactivated subvirion vaccine that incorporated the HA from A/Vietnam/1203/2004 (VN/1203) H5N1 clade 1 influenza virus. After 22 months, the individual was boosted with a monovalent inactivated influenza A vaccine containing the HA and NA of A/Anhui/01/2005 (H5N1). The volunteer subsequently received a subunit vaccine containing monovalent inactivated influenza A/Shanghai/02/2013 (H7N9). For the current study, the donor was vaccinated with a 2014 to 2015 seasonal trivalent inactivated influenza vaccine on day 0. Peripheral blood samples were obtained on days 0, 3, 4, 5, 6, 7, 10, 11, 14, and 31 after immunization.

Peripheral blood mononuclear cells (PBMCs) from day 31 after vaccination were immortalized by EBV transformation, and the supernatants were screened for the presence of Abs with binding to recombinant HA proteins derived from H1 (A/California/04/2009, A/Texas/36/1991), H3 (A/Hong Kong/1/1968, A/Victoria/3/1975), H7 (A/Shanghai/2/2013, A/Netherlands/219/2003), and H9 (A/Hong Kong/1073/99) subtypes by ELISA. The hybridoma cell line secreting the FluA-20 mAb was made from a B cell line that exhibited heterosubtypic breadth. Two additional broadly reactive non-neutralizing heterosubtypic mAbs, designated FluA-45 and FluA-55, also were isolated and used in these studies for comparative purposes.

Deep sequence analysis of Ab variable gene sequences in circulating PBMCs in the donor revealed sequences that were clonally related to FluA-20 (i.e., "siblings"), defining two sequences as clonally related if they used the same V_H and J_H gene and differed by 3 or fewer amino acids in the heavy chain complementarity-determining region 3 (HCDR3) region. We identified siblings of FluA-20 in blood samples from 4 time points: days 5, 6, 11, and 14 post vaccination with trivalent inactivated influenza vaccine (TIV). The majority of these siblings arose from one common ancestor and formed 3 major clusters (designated A, B, and C) that differ by point mutations (Figure 1B). Network analysis suggested that FluA-20 arose from cells present at day 6 that also were observed at day 14 (Figure 1B).

Binding Profile of FluA-20 and Sibling Ab with Various Subtypes of Influenza Type A HA Molecules

FluA-20 exhibited extraordinary binding breadth and affinity to recombinant HA timers belonging to group 1 and group 2 viruses, with half maximal effective concentration (EC_{50}) values in ELISA for binding ranging from 5 to 142 ng/mL (Figures 1C and S1A). A recombinant form of FluA-20 IgG protein was expressed; hybridoma-generated Ab (designated FluA-20) was used for the assays unless the recombinant form is specified (designated as rFluA-20). The rFluA-20 IgG showed a similar binding spectrum to the hybridoma-produced FluA-20 IgG protein (Figures 1C and S1A). Also, we recombinantly expressed FluA-20 as an Fab and assessed its kinetics of binding to representative HA subtypes (Table S1). The rFluA-20 Fab interacted with most HA molecules from H1, H2, H3, H5, and H7 subtypes with K_D values less than 100 nM (with several less than 1 nM; Table S1).

(C) ELISA binding EC_{50} (ng/mL) values for FluA-20, recombinant FluA-20 (rFluA-20), and unmutated common ancestor of FluA-20 (FluA-20-UCA) to HAs derived from different strains representing group 1 (green) and group 2 (blue) IAVs. The table is displayed in purple-white color scale corresponding to strong-weak binding, respectively. The > symbol indicates that binding was not observed at concentrations ≤10 μg/mL.
See also Figure S1.

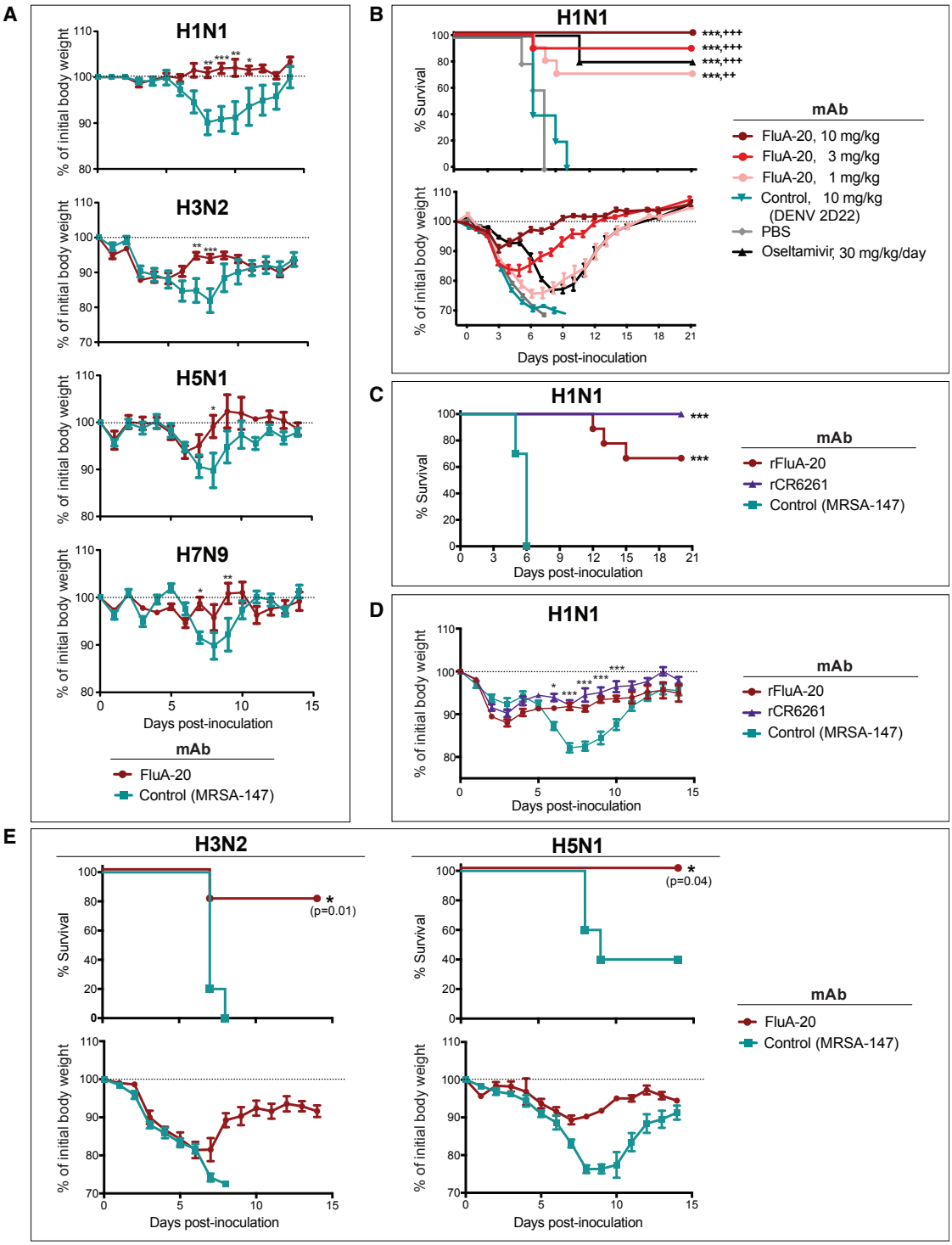

Figure 2. MAb FluA-20 Exhibits Protection *In Vivo* against Diverse IAV Subtypes

(A) Body-weight change in mice that received FluA-20 prophylactically prior to sub-lethal challenge with IAV strains from H1N1, H3N2, H5N1, or H7N9. Mice were treated with 10 mg/kg of either FluA-20 or a similarly prepared control Ab to an unrelated target and challenged 24 h later with either H1N1 A/Netherlands/602/2009 or H3N2 A/X-31 (6:2 PR8 backbone) or H5N1 A/barn swallow/Hong Kong/D10-1161/2010 (7:1 PR8 backbone) or H7N9 A/Shanghai/1/2013 (6:2 PR8 backbone). The weight loss of mice (n = 5) was measured daily for 14 days after inoculation (day 0). The experiments were performed twice with similar results.

(legend continued on next page)

We also recombinantly expressed and tested somatic variant (sibling) Abs related to FluA-20 from cluster A and cluster B (Figure S1B). Three sibling Abs, Sibs 2, 3, and 45, had very similar activity and breadth to rFluA-20 (Table S2). Also, two sibling Abs, Sibs 28 and 48, in a phylogenetic cluster that was more mutated than FluA-20, lost binding to some H3, H5, and H14 HAs, and Sibs 7 and 33 lost activity to any HA tested (Table S2). Thus, the FluA-20 clonotype contains multiple variants with a diverse breadth of reactivity.

Unmutated Common-Ancestor-Origin Interactions Drive the Activity of the FluA-20 Lineage

FluA-20 is from the IgG1 subclass and is encoded by the V_H4-61/D2-15/J_H4 and V_K1-39/J_K1 variable gene segments, which represent a genetic configuration not previously reported for broadly reactive human influenza Abs. The FluA-20 cDNA sequence shares 93% identity with both the V_H4-61*01 and V_K1-39*01 germline genes. Compared to the inferred unmutated common ancestor (UCA) sequence (FluA-20-UCA), FluA-20 has 16 somatic mutations in the heavy-chain amino-acid sequence and 11 in the light chain (Figure S1C). Recombinantly expressed IgG or Fab FluA-20 UCA Abs retained the substantial binding breadth of rFluA-20 (Figures 1C and S1A; Table S1). Nonetheless, compared to the UCA Ab, rFluA-20 displayed not only an increase in binding potency but also greater breadth with additional recognition of many H3 and H5 HAs.

FluA-20 Exhibits Prophylactic and Therapeutic Efficacy *In Vivo* Against Viruses of Diverse IAV Subtypes

Sublethal Influenza Mouse Model of Ab Prophylaxis

We chose A/Netherlands/602/2009 (H1N1), A/X-31 (H3N2), A/barn swallow/Hong Kong/D10-1161/2010 (H5N1), and A/Shanghai/1/2013 (H7N9) virus strains, representative of group 1 and group 2 IAVs, for prophylactic studies. BALB/c mice (n = 8 per group) were administered 10 mg/kg of FluA-20 IgG or a similarly prepared control Ab by the intraperitoneal route, then challenged 24 h later intranasally with a sublethal dose of virus. Mice treated with FluA-20 (n = 5) showed complete protection from weight loss after H1N1 challenge (Figure 2A), whereas mice challenged with H3N2, H5N1, or H7N9 strains showed significantly faster recovery from weight loss compared to control animals (Figure 2A). Additionally, FluA-20 treatment reduced lung titers (day 6 post inoculation) after H1N1 or H7N9 challenge (Figure S2A).

Lethal Influenza BALB/c Mouse Model of Ab Prophylaxis Using Mouse-Adapted H1N1 Virus

To further evaluate the optimal dose of FluA-20 for prophylactic efficacy, we tested 3 different doses of FluA-20 against lethal challenge with mouse-adapted H1N1 A/California/04/2009 virus. BALB/c (n = 10 per group) mice were injected i.p. with 1, 3, or 10 mg/kg of FluA-20 or 10 mg/kg of a control Ab or PBS 14 h prior to intranasal challenge with H1N1 virus. As a control, one experimental group was treated with the commercially available IAV drug oseltamivir twice daily for 5 days, starting at 1 h post inoculation. Remarkably, FluA-20 provided significant protection against mortality and protection against severe weight loss at all 3 tested doses, with groups that received 3 or 10 mg/kg showing better efficacy than groups with oseltamivir (Figure 2B).

Lethal Influenza DBA/2J Mouse Model of Ab Prophylaxis Using Human H1N1 Virus

We also evaluated mAb FluA-20 for prophylactic efficacy against lethal challenge with non-mouse-adapted H1N1 A/California/04/2009 virus in DBA/2J mice and observed significant protection in FluA-20-treated mice (10 mg/kg) compared to mice given control IgG (Figure 2C).

Sublethal Influenza BALB/c Mouse Model of Ab Therapy Using Human H1N1 Virus

To determine the therapeutic potential of FluA-20, we measured protection against weight loss after sublethal challenge of mice with human H1N1 virus. Mice treated with mAb FluA-20, similarly to mice treated with positive control mAb CR6261, showed significant protection against severe weight loss and faster recovery (days 6 to 10 post challenge) when compared to mock-treated mice (Figure 2D).

Lethal Influenza BALB/c Mouse Model of Ab Therapy Using H3 and H5 Viruses

We also tested efficacy of mAb FluA-20 treatment in a lethal model by measuring survival, weight loss, and lung virus titers in BALB/c mice (n = 5 per group) that were lethally challenged with H3N2 or H5N1 viruses on PR8 backbone and treated the next day with FluA-20 or control mAb (Figures 2E and S2B). Treatment with mAb FluA-20 showed a significant protection from mortality (Figure 2E). Collectively, these results indicate the ability of FluA-20 to protect prophylactically and therapeutically *in vivo* against sublethal or lethal virus challenge against influenza A virus strains of diverse subtypes.

FluA-20 IgG Does Not Compete for Binding to HA with Other RBS- or Stem-Specific Abs

We used bio-layer interferometry to measure if FluA-20 competed for HA binding against other known bnAbs. FluA-20 did not compete for binding to HA with RBS-mAbs (mAb 5J8) or stem-specific mAbs (mAbs CR9114, FI6v3, 39.29, and H3v-86) (Figure S3A). Also, FluA-20 interacted well with truncated

(B) Survival and weight change in mice (n = 10) prophylactically treated with FluA-20 (1 or 3 or 10 mg/kg) or 10 mg/kg of control IgG or PBS prior to lethal challenge with mouse-adapted H1N1 A/California/04/2009. One experimental group was treated with 30 mg/kg/day of oseltamivir for 5 days post challenge as a positive control. ***p < 0.001, compared to placebo-treated group; +++p < 0.001, ++p < 0.01, compared to Dengue virus (DENV) 2D22-treated group.

(C) Percentage survival in mice prophylactically treated with 10 mg/kg of either FluA-20 or a recombinant form of CR6261 or control IgG (MRSA-147) prior to lethal challenge with H1N1 A/California/04/2009 virus.

(D) Weight change in mice that were sub-lethally challenged with H1N1 A/California/04/2009 virus prior to therapeutic treatment with 10 mg/kg of either mAbs FluA-20 or a recombinant form of CR6261 or control IgG (MRSA-147) on day 1 post-inoculation.

(E) Survival and weight change in mice lethally challenged with H3N2 and H5N1 viruses (same strains as A) prior to therapeutic treatment with 10 mg/kg of either mAbs FluA-20 or control IgG on days 1, 2, and 4 post inoculation. Each group was compared to the mock-treated group in (A) to (E). Body-weight-change data in (B) and (E) are shown only for the animals that survived at each indicated time point. The weights in (A), (B), (D), and (E) are shown as the group mean and the SEM. See also Figure S2.

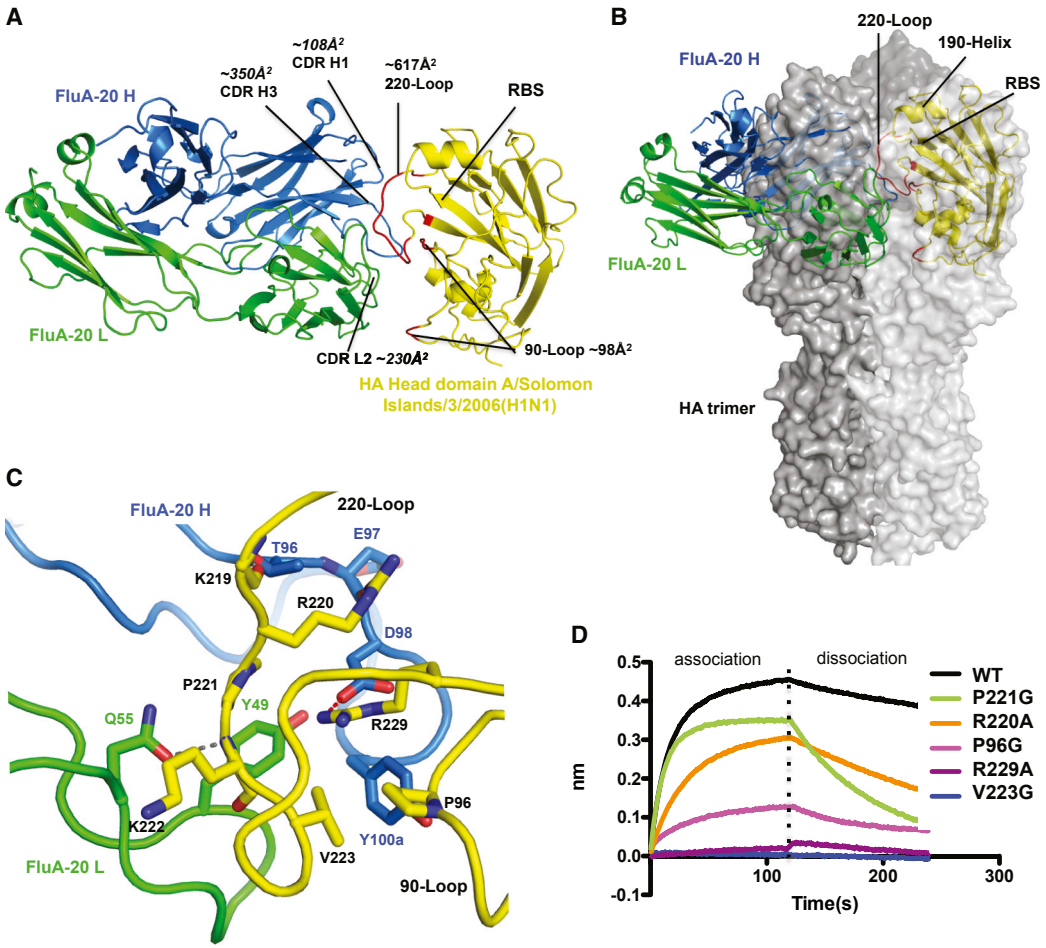

Figure 3. FluA-20 Targets the 220-Loop and the 90-Loop at the Trimer Interface of the H1 Head Domain

(A) Structural overview of rFluA-20 Fab in complex with the head domain of H1 HA (A/Solomon Islands/3/2006). FluA-20 Fab is shown as a backbone trace in blue heavy chain (H) and green light chain (L). The backbone of the HA head domain is shown as a yellow trace and residues contacted by FluA-20 are red.

(B) The H1 head domain is superimposed with one protomer colored in light gray surface from an HA trimer structure (PDB: 4M4Y). The adjacent HA protomers are shown with a dark gray solid surface. The variable domain of FluA-20 would clash with a large area of the head domain from an adjacent protomer in the HA trimer model.

(C) FluA-20 interaction with H1. The salt bridge interaction between Asp98 (H) to Arg229 is shown as a red dashed line. A hydrogen bond between Asn55 (H) to Lys222 is indicated with a gray line. Two additional hydrogen bonds are between the side chain of Thr96 (H) to main-chain carbonyl of Lys219 and Arg220 side chain to the main-chain carbonyl of Glu97 (H). Other hydrophobic residues that contribute to the interaction are shown with side chains.

(D) The binding traces of HA head domain or its mutants (at the concentration of 0.5 μM) to immobilized rFluA-20 Fab in bio-layer interferometry (BLI) assay are presented.

See also Figures S3 and S4.

HA head domains lacking the stem region, derived from multiple HA subtypes (Figure S3B). These data indicated that FluA-20 recognizes a distinct protective epitope on the HA head domain that is conserved across most IAVs.

Structural Characterization of FluA-20 in Complex with the HA Head from H1 A/Solomon Islands/3/2006 Reveals a Novel Epitope at the Trimer Interface

To identify this novel site of vulnerability on the HA head, crystal structures of the apo form of rFluA-20 Fab and its complex with the HA head domain from A/Solomon Islands/3/2006 (H1N1) were determined at 1.73 Å and 2.85 Å resolution, respectively (Tables S3 and S4). Two HA head domains, each bound by one Fab, were present in the crystal asymmetric unit.

The complex structure revealed that FluA-20 recognizes an epitope that is adjacently lateral to, but does not overlap with, the RBS (Figure 3A). The Ab interacts primarily with the 220-loop and has some contact with the 90-loop, creating buried surface areas of 617 $Å^2$ and 98 $Å^2$ on each loop. After superimposing the HA head domain in the Fab complex with an H1 HA trimer structure (PDB: 4M4Y), the FluA-20 epitope was found to be hidden in the HA trimer interface and inaccessible for Ab binding in the conventional HA trimer configuration (Figure 3B). In fact, the non-RBS side of 220-loop is an important surface

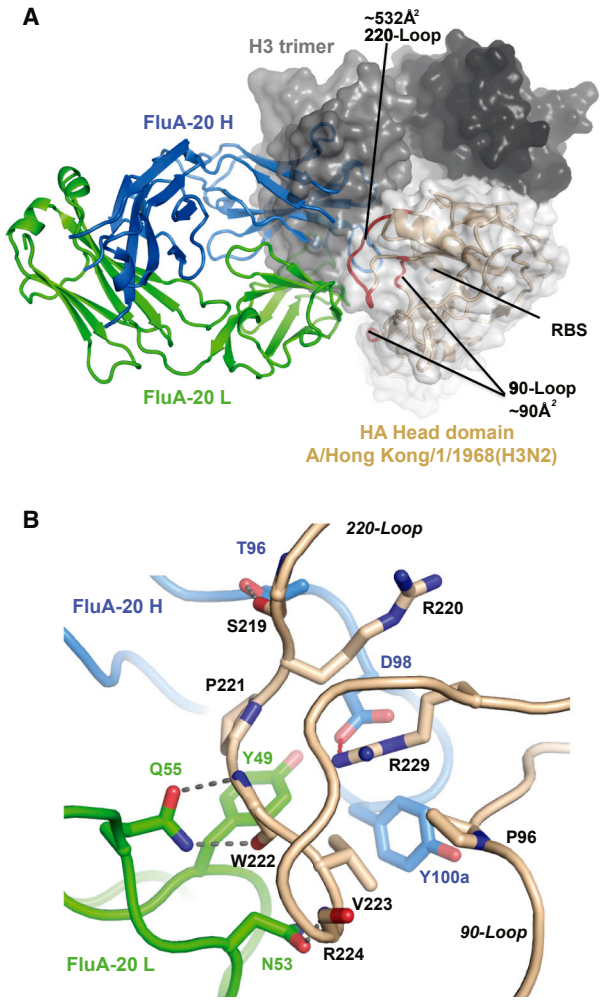

Figure 4. FluA-20 Interacts with H3 Head Domain

(A) The structure of rFluA-20 in complex with a H3 head domain (A/Hong Kong/3/1968) is presented similarly to Figure 3, with the H3 head domain colored in wheat. The H3 residues interacting with FluA-20 are red and the Ab footprint size on HA is analyzed. The H3 head domain is superimposed with one protomer of an H3 trimer structure (PDB: 4FNK; shown as surface with different shade of gray for each protomer).

(B) Interaction of FluA-20 with H3 HA. A salt bridge between R229 from HA and Asp98 (H) of FluA-20 is shown with a red line. Hydrogen bonds between Gln55 (L) to main chain of Trp222 and Asn53 (L) to Arg224 are presented with gray dashed lines. Several hydrophobic residues that contribute to the interaction are shown with their side chains.

See also Figure S4.

for interaction of the HA with its adjacent protomer in the native trimer (Figures S4A and S4B). The variable domain of FluA-20 on the monomeric head domain then overlaps with the head domain from an adjacent protomer in the HA trimer structure (Figure 3B). These results suggested that FluA-20 recognizes HA in a form different from the canonical closed trimer structure.

The interaction of FluA-20 with HA is mediated mainly by a groove between CDRs H3 and L2, with some contacts from CDR H1 to the edge of its epitope (Figure 3A). Many contacts of FluA-20 with HA are centered on Arg229 (Figure 3C). First, Asp98 (H) of FluA-20 makes a salt bridge with Arg229 (Figure 3C). Surrounding this salt bridge is an enclosed hydrophobic pocket formed by both HA and FluA-20 residues, including Pro221, Val223, and Pro96 of HA and Tyr49 (L) and Tyr100a (H) of FluA-20 (Figure 3C). The aromatic ring of Tyr100a (H) of FluA-20 is positioned approximately 4 Å away from the basic amine of Arg229 in HA and likely forms cation-π interactions that would strengthen the binding. Alanine mutation of Arg229 completely abolished binding of FluA-20 to the HA (Figure 3D). Glycine mutation of Val223 or Pro96 in the HA epitope also substantially decreased HA binding by FluA-20, indicating that these hydrophobic contacts between the non-polar residues in HA to Tyr49 (L) and Tyr100a (H) of FluA-20 are important for its activity (Figure 3D). Reciprocally, D98A (H) or Y49A (L) mutants of FluA-20 disrupted binding to all targeted HAs, and an alanine mutation of Tyr100a (H) in FluA-20 also eliminated binding to most HA subtypes (Table S5).

Several hydrogen bonds also are involved in the binding of FluA-20 to HA. The side-chain amine of HA Arg220 hydrogen bonds to the main-chain carbonyl of Glu97 (H) from the Ab (Figure 3C). Additionally, the Gln55 (L) side-chain carbonyl interacts with the main-chain amide of Lys222 on the HA (Figure 3C). As a result, mutation of either HA Arg220 or Gln55 (L) of FluA-20 decreases the binding interaction (Figure 3D; Table S5).

Structural Characterization of FluA-20 in Complex with the HA Head of H3 A/Hong Kong/1/1968

We also determined the crystal structure of rFluA-20 Fab in complex with the HA head domain of A/Hong Kong/1/1968 (H3N2) at 2.10 Å resolution (Table S4). Each asymmetric unit includes one FluA-20 in complex with one H3 head domain. FluA-20 interacts with a similar epitope on the H3 head domain as with H1, with similar interactions (Figures 4A, S4C, and S4D). The structural alignment of the H3 head domain bound by FluA-20 with the H3 trimer model (PDB: 4FNK) again indicated that the Ab interacts with HA in a form other than the canonical trimer (Figure 4A).

Additional hydrogen bonds are made between the side-chain amine of Gln55 (L) of FluA-20 to the main-chain carbonyl of Trp222 in HA and the Asn53 (L) side-chain carbonyl to the Arg224 main-chain amide (Figures 4B and S4B). Gln55 (L) appears to be important for FluA-20 binding to many other HA strains, although not for H3 (A/Hong Kong/1/1968) and a few other strains (Figure 4B; Table S5). The interaction by Asn53 (L) is not required for Ab binding to most HAs (Table S5).

Hydrogen Deuterium Exchange Mass Spectrometry (HDX-MS) Experiments Confirm Interaction of the FluA-20 with the H5 HA Trimer Interface

To confirm that FluA-20 interacts with the equivalent epitope on H5 HA, we conducted hydrogen deuterium exchange mass spectrometry (HDX-MS) experiments with a monomeric head domain of H5 (VN/1203) to identify peptides on the surface of HA that are occluded following binding of FluA-20. FluA-20 blocked labeling of peptides comprising residues 210 to 223 (Figures S5A and S5B), consistent with the location of the epitope in the co-crystal structures with the subtype H1 or H3

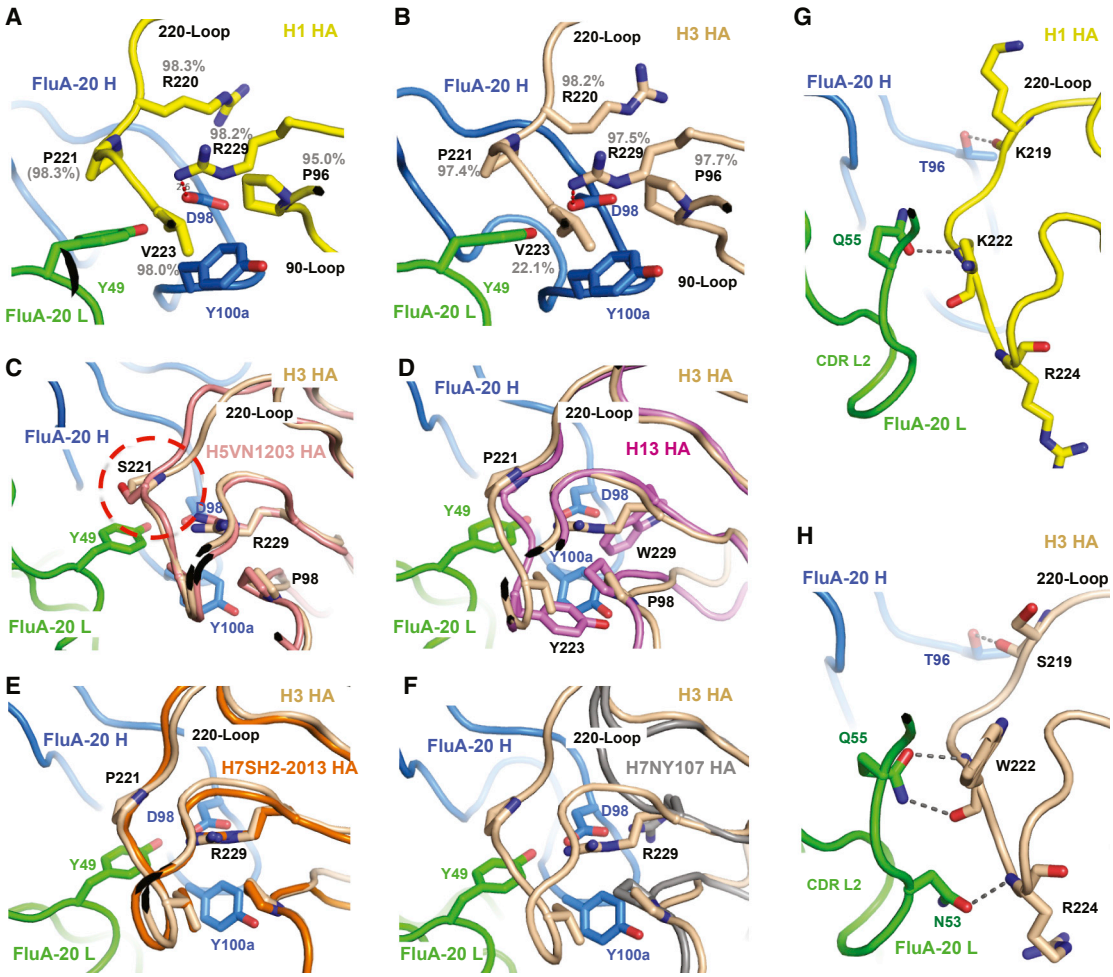

Figure 5. Critical Residues Involved in FluA-20 Binding to Different HAs

(A and B) Principal residues that FluA-20 recognizes in HA head domains are highly conserved across various HA subtypes. The binding core of FluA-20 in complex with H1 (A) or H3 (B) HA is highlighted by a salt bridge between Asp98 (H) and Arg229, which is enclosed by a circle of hydrophobic residues, including Pro96, Pro221, and Val223 of HA and Tyr49 (L) and Tyr100a of FluA-20. The conservation of the core residues in each HA subtypes is indicated by identity percentages.

(C–F) Simulation of FluA-20 binding to HAs from other subtypes. The head domains of H5 (C), H13 (D), or H7 HA (E and F) are superimposed with H3 HA (colored in wheat) in complex with FluA-20. (C) H5 (VN/1203) has Ser221 (red circle), instead of Pro221 in H1 and H3 subtypes. The K_D values of FluA-20 Fab binding to either wild-type (WT) H5 or H5_S221P mutant were determined by BLI assay; the WT K_D was 122 nM and the S221P K_D was 15 nM. (D) Instead of the salt bridge interaction between Asp98 (H) of FluA-20 and Arg229 in other HAs, H13 HA possesses two aromatic residues, Tyr223 and Trp229, that contribute to the binding by aromatic stacking with Y100a. (E) H7 HA of A/Shanghai/2/2013, in orange, aligns well to H3_FluA-20 complex structure. (F) H7 HA of A/New York/107 /2003 (gray) was aligned to the H3_FluA-20 complex structure. This H7 strain has a truncated 220-loop and is missing residues 221 to 228.

(G and H) FluA-20 accommodates variability in the HA 220-loop of H1 (G) or H3 (H) HA. Residues 219, 222, and 224 in the FluA-20 epitope exhibit considerable variation in various subtypes. However, FluA-20 forms hydrogen bond interactions with the main chains of these variable residues (in gray lines), and the approach angle of FluA-20 successfully avoids contacts or collisions with bulky and variable side chains.

See also Figure S5.

HAs. Single mutants of R220A, V223A, or R229A in the 220-loop of H5 HA completely abolished FluA-20 binding, confirming that the Ab uses a similar binding mechanism for H5 as those observed for H1 and H3 (Figure S5C).

The FluA-20 Epitope Is Highly Conserved across Different Subtypes of IAV HA

The five HA residues with which FluA-20 primarily interacts, namely Pro96, Arg220, Pro221, Val223, and Arg229, are highly conserved among all human H1N1 viruses (95% conservation for Pro96 and over 98% conservation for the other four residues) (Figure 5A). In human H3N2 viruses, conservation of key residues in the epitope is generally above 97%, except for residue 223. Approximately 22% of H3 strains encode Val223, including A/Hong Kong/1/1968 (H3N2) (Figure 5B), but 70% of H3 HAs possess Ile223. Two strains of H3 with the Ile223 variant, A/Texas/50/2012 and A/Switzerland/9715293/2013, were tested in the activity profiling, and both bind to FluA-20 with high affinity.

Thus, FluA-20 can effectively accommodate either Val or Ile at HA1 position 223.

The sequences of the major epitope residues recognized by FluA-20 in other HA subtypes are summarized in Table S6. The five major epitope residues (P96 [structurally conserved although numbered differently in various HA subtypes], R220, P221, V/I223, and R229) that directly interact with FluA-20 remain highly conserved across different strains and subtypes, which explains the extraordinary breadth of FluA-20. Some mutations or deletions in these five key residues in the epitope of a few HAs may inhibit binding to FluA-20. For instance, Arg229 is essential for electrostatic interactions with FluA-20 (Table S6; Figures 5A and 5B). An Ile229 substitution in H3 A/Minnesota/11/10 likely renders it the only H3 strain that FluA-20 fails to recognize among those tested, whereas a Trp229 residue in H13 (A/gull/Maryland/704/1977) can be tolerated. Comparison of the H13 structure (PDB: 4KPQ) with the H1 or H3 complexes with FluA-20 shows that H13 possesses a unique pair of mutations, Tyr223 and Trp229 (Figure 5D). Possible aromatic stacking of these two residues with Tyr100a (H) of FluA-20 may compensate for the loss of the Arg229 contacts.

Compared to H1 and H3, two H5 strains with Ser221 (a common substitution in the H5 subtype) exhibited weaker binding of FluA-20 (Figure 5C). Ser221 does not appear to change the 220-loop conformation (Figure 5C); however, the decrease of side-chain hydrophobicity or difference in the rigidity of the 220-loop may have affected FluA-20 binding. In fact, a Pro221 mutation in H5 (VN/1203) substantially rescued the affinity to FluA-20 to a level similar to that of H1 or H3 (Figure 5C). Of the two H7 strains tested, the H7 HA of A/New York/107/2003 has a truncated 220-loop (missing residues) but still retains the critical Arg229. As a result, this H7 HA shows decreased binding by FluA-20 compared to H7 from A/Shanghai/2/2013 (Figures 1C, 5E, and 5F). Considerable variation nevertheless exists at some residues in the FluA-20 epitope, particularly for 219, 222, and 224, that are located very close to the epitope binding core. However, the interactions of FluA-20 with these variable residues are only to their main chain, and the approach angle of FluA-20 enables the Ab to successfully accommodate these variable side chains (Figures 5G and 5H).

Mutation Experiments Confirm the Critical Contact Residues in the FluA-20 IgG Paratope

To determine the paratope residues that are critical for FluA-20 binding, we mutated Tyr34, Thr96, Glu97, Aps98, Tyr100a, or Cys101 on the heavy chain (H) and Tyr49, Asn53, or Gln55 on the light chain (L) to alanine and recombinantly expressed each variant to determine relative binding to HAs from different subtypes compared to rFluA-20. Two mutants, D98A (H) and Y49A (L), showed complete loss of binding to all tested HAs, validating the importance of the electrostatic interaction between Asp98 (H) of FluA-20 and Arg229 on HA and the hydrophobic interaction between Tyr49 (L) to HA residues (Table S5; Figures 5A and 5B). Furthermore, Q55A (L) mutant showed >10-fold or complete loss of binding EC_{50} to all HAs except H1 A/Texas/36/1991, H3 A/Hong Kong/1/1968, and H7 A/Netherlands/219/2003, whereas the Y100aA (H) mutant also showed >10-fold loss of binding EC_{50} to all HAs except H3 A/Hong Kong/1/1968 (Table S5). Additionally, C101A (H) or N53A (L) also disrupted binding to H5 A/Indonesia/5/2005 HA. Collectively, these findings indicate that, although the binding core of the FluA-20 interaction with different HAs is highly conserved, some variations can occur with different HAs. These findings are also consistent with our observation that the FluA-20-UCA, which carries the key HA-contacting residues Asp98 (H), Y100a (H), Y49 (L), and Gln55 (L), retains much of the binding breadth compared to FluA-20 (Figures 1C and S1C).

Binding of FluA-20 to HA Is Inhibited by HA Cleavage, Likely through Dynamic Changes in the HA Trimer

During viral replication, HA is synthesized initially as a precursor protein, HA0. As the protein folds, HA assembles into a trimer in the endoplasmic reticulum before its transportation to the cell surface (Copeland et al., 1986; Gething et al., 1986). HA0 can be cleaved post-translationally at an arginine (or, rarely, a lysine) around residue 329 into two subunits, HA1 and HA2, the mature form of HA. HA cleavage is a prerequisite for viral infectivity (Chen et al., 1998; Steinhauer, 1999).

We observed that trypsin cleavage of HA substantially decreased binding of FluA-20 to soluble H1 or H7 HA (Figure 6A), whereas differences in binding of the RBS-binding Abs were not observed after cleavage (Figure S7G). Because the FluA-20 epitope is buried in the HA trimer interface, the biased inhibition of FluA-20 binding, but not the "outer" surface binding Abs, suggests a potential decrease of dynamics in the HA trimer after trypsin treatment. The FluA-20 epitope in the trimer interface may be less frequently or less proportionally exposed after the HA cleavage. We also assessed FluA-20 binding to cell-surface HA and tested whether the surface HA recognition is affected by trypsin treatment. We performed flow cytometric analysis to measure binding of two Abs, CR9114 or FluA-20, to H3 A/Hong Kong/1/1968 HA expressed on HEK293F cells, either untreated or treated with trypsin. Consistent with our observations with soluble, recombinant HA protein, FluA-20 displayed substantially lower binding to HA on trypsin-treated cells compared to untreated cells (2.6-fold), whereas a decrease of the stem Ab CR9114 binding was not observed after trypsin treatment (Figure 6B).

To examine if this specificity of FluA-20 for uncleaved HA is due to better epitope accessibility in the uncleaved form, we performed an HDX-MS experiment with either HA0 or trypsin-treated HA trimers to compare their trimer dynamics. Indeed, we observed an overall reduction of deuterium exchange in the cleaved HA molecules compared to HA0 proteins at the three time points tested, except for some loops near the vestigial esterase subdomain of HA head (Figures 6C and S6C). In summary, these data suggest that HA cleavage into its functional form reduces HA trimer dynamics, which may inhibit exposure of the FluA-20 epitope in the matured, functional form of HA on virions.

FluA-20 Inhibits Cell-to-Cell Spread, Potentially by Disrupting Native HA Trimers

FluA-20 did not exhibit neutralizing activity when tested by hemagglutinin inhibition assay (HAI) or microneutralization assays against H1N1 A/California/04/2009, H3N2 A/Texas/50/2012, or H7N9 A/Shanghai/2/2013 (6:2 PR8 backbone) viruses. We also performed microneutralization assays with uncleaved HA0 virus

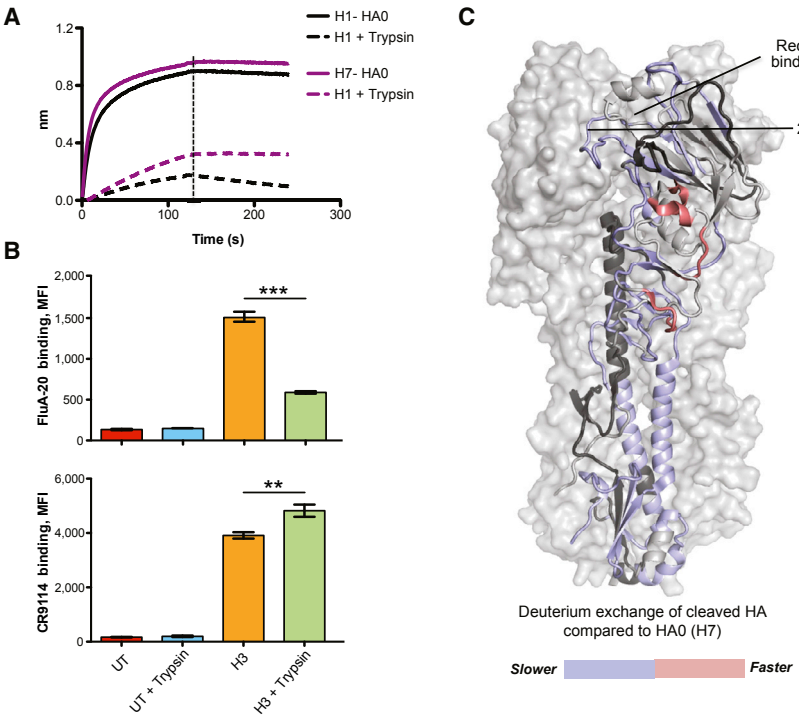

Figure 6. FluA-20 Binding Is Inhibited by HA Cleavage Potentially Due to Dynamic Changes in the Trimer

(A) The association and disassociation traces of HA0 trimer or cleaved HA trimer from H1 (A/California/04/2009) or H7 (A/Shanghai/02/2003) to immobilized rFluA-20. The HA was tested at 1 μM concentration.

(B) HEK293F cells were either untransfected (UT) or transiently transfected with full-length H3 (A/Hong Kong/1/1968) HA cDNA for HA surface expression. The cells were either left untreated or treated with N-tosyl-L-phenylalanine chloromethyl ketone (TPCK) trypsin and then incubated with 10 μg/mL of mAb CR9114 or mAb FluA-20 followed by incubation with secondary Ab. Ab binding to cleaved and uncleaved HA on the cell surface was determined by flow cytometric analysis. The error bars represent mean ± SD of technical replicates. Statistical significance was calculated using the unpaired two-tailed t test. Data are representative of two independent experiments.

(C) Deuterium exchange comparison of cleaved HA trimer to HA0 trimer from A/Netherlands/219/2003 (H7N7) by HDX-MS. One HA protomer in the model (PDB: 4DJ6) is shown in colored backbone trace. Peptides with slower deuterium exchange in cleaved HA are blue, and peptides with faster exchange are red. Peptides in gray represent no difference in deuterium exchange rate, and peptides in black indicate peptides that were not covered in the MS data.

See also Figure S6.

(H3N2 A/Hong Kong/1/1968) to test the effect of HA cleavage on susceptibility to neutralization by FluA-20. Although FluA-20 binds HA0 to a higher extent than its cleaved form, it did not neutralize HA0 virus (virus produced in the absence of trypsin) (Figure S6B). Consistent with the absence of neutralizing activity, FluA-20 did not block trypsin-mediated cleavage of HA (Figure S7A) or inhibit the pH-dependent conformational change of HA (Figure S7B). However, when tested for neutralization activity in plaque assay with H3N2 A/Hong Kong/1/1968 virus, FluA-20 showed a 3.8-fold reduction in the plaque size compared to the control Ab, as measured by the % foci area per well (Figures 7A and 7B). FluA-20 showed a dose-dependent inhibition of cell-to-cell spread of the virus with inhibitory activity comparable to that of broadly neutralizing Ab CR9114 (Figures 7A, 7B, and 7C). Zanamivir, a neuraminidase inhibitor that functions by blocking viral egress, displayed efficient inhibition of cell-to-cell virus spread and was used as a positive control. To examine if FluA-20 reduced spread by inhibiting viral egress, we performed an egress inhibition assay with H3N2 A/Texas/50/2012 H3N2. FluA-20 did not inhibit egress, whereas mAb H3v-47 (which has been previously shown to have egress inhibition activity comparable to that of zanamivir; Bangaru et al., 2018) showed potent egress inhibition (Figure S7C). Collectively, these results indicate that FluA-20 inhibits IAV in a novel mechanism by binding of mAb FluA-20 to the HA trimer interface and blocking cell-to-cell spread.

Fc-mediated ADCC activity has emerged as a mechanism by which some broadly reactive influenza Abs confer *in vivo* protection (DiLillo et al., 2016, 2014). To examine if FluA-20 also could mediate ADCC activity, we performed an ELISA-based screen using recombinant soluble (rs), dimeric, low-affinity ectodomains (rsFcγR) of FcγRIIIa (Wines et al., 2016). These rsFcγR low-affinity dimers require simultaneous engagement of both receptors by HA-bound IgGs to achieve stable binding in ELISA. Four similarly prepared Abs, FluA-20, FluA-45, FluA-55, or VRC01 (an HIV-reactive negative control mAb) were added to plates coated with H1 A/California/04/2009 HA to test for their ability to engage both binding sites on rsFcγR simultaneously (Kristensen et al., 2016). The FluA-20 IgG strongly engaged the rsFcγR dimers, whereas neither the HA-reactive mAbs FluA-45 and FluA-55 nor the HIV-specific control mAb VRC-01 engaged these FcγR molecules (Figure S7D). We next examined the ability of these Abs to activate primary $CD3^-$ $CD56^+$ natural killer (NK) cells following incubation with HA from A/California/04/2009 *in vitro* (Jegaskanda et al., 2013). NK-cell activation was measured as the percentage of NK cells expressing intracellular IFN-γ and/or CD107a (markers for degranulation) (Al-Hubeshy et al., 2011; Alter et al., 2004). A robust concentration-dependent increase of NK-cell activation was observed for FluA-20 (1.3%, 9.2%, or 14.6% NK-cell activation at 0.1, 1, or 10 μg/mL FluA-20, respectively), whereas FluA-45, FluA-55, and HIV mAb VRC01 did not exhibit any NK-cell activation (Figure S7E). To further investigate if this activity contributes to protection *in vivo*, we engineered two separate Fc mutant variants, N297A or L234A/L235A (LALA), in the FluA-20 IgG1 sequence. Introduction of these mutations in IgG Fc reduces or abrogates binding of Fc to both human and mouse FcγRs (Arduin et al., 2015; Chao et al., 2009; Hezareh et al., 2001; Morgan et al., 1995). We compared the

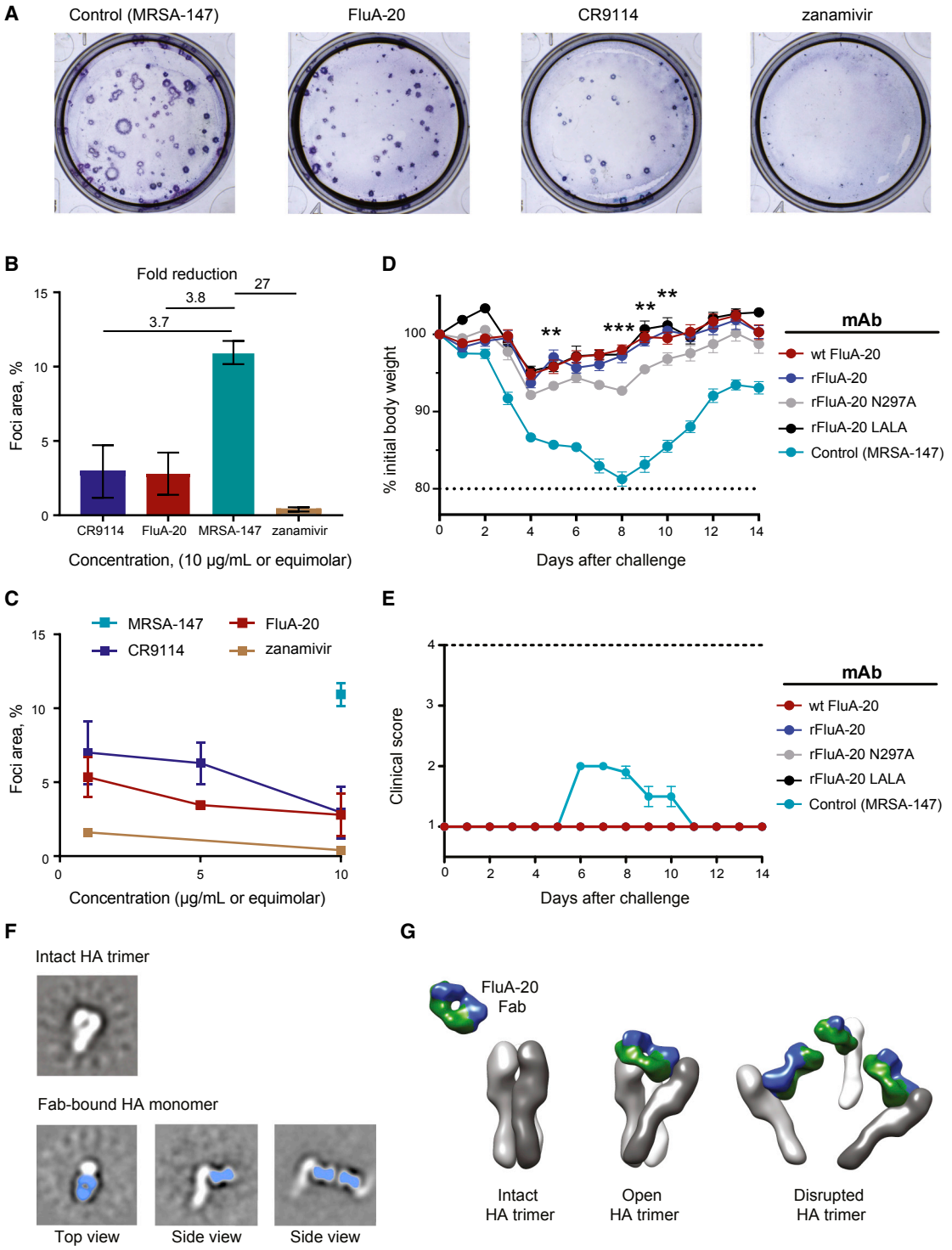

Figure 7. FluA-20 Inhibits Cell-Cell Spread, Disrupts the Uncleaved HA Trimer Protein, and Does Not Require Fc-Effector Function for *In Vivo* Protection

(A–C) demonstrate that FluA-20 diminishes cell-to-cell spread of influenza virus. (A) Representative images of 6-well plate wells with influenza virus A/Hong Kong/1/1968 foci developed on Madin-Darby canine kidney (MDCK) monolayers after 48 h of incubation at presence of 10 μg/mL of irrelevant control mAb MRSA-147, FluA-20, CR9114, or equimolar concentration of zanamivir; foci were immunostained and images were captured by CTL (Cellular Technology). Images are representative of 3 replicates of 2 independent experiments. (B) Quantitative determination of foci area reduction. Foci area calculated by ImageJ

(legend continued on next page)

protective efficacy of FluA-20 Fc variants with recombinant and hybridoma-derived FluA-20 by measuring weight loss and clinical score in BALB/c mice that were injected prophylactically with 10 mg/kg of mAb 24 h prior to challenge with 1.2×10^4 focus forming units (FFU) of H1N1 A/California/04/2009 virus. The virus titer optimal for challenge studies was determined initially by challenging animals with different titers of virus (Figure S7F). Surprisingly, both Fc variants exhibited significant protection against the H1N1 challenge compared to the control Ab (Figure 7D). Although mice treated with the N297A Fc variant Ab demonstrated significant differences in weight loss compared to rFluA-20, we did not observe a significant impact on the overall protection (Figures 7D and 7E). Taken together, these results indicate that, although FluA-20 has the ability to robustly activate NK cells *in vitro*, the Fc-mediated ADCC activity is dispensable for its protective role *in vivo*.

From the structural studies, it is apparent that FluA-20 binding to the HA trimer should destabilize the trimeric interface of native HA. To directly examine the effect of FluA-20 binding to trimer, we performed negative-stain electron microscopy (nsEM) of FluA-20 Fab-HA (uncleaved H1 A/California/04/2009) complexes incubated at various time points. Native H1 HA0 trimer remained in its trimeric conformation during nsEM sample preparation (Figure S7G). In contrast, we observed that, upon exposure to FluA-20 even for 20 seconds (the shortest time point that could be tested), the HA0 trimers quickly transformed to Fab-bound monomeric HA, with only a small fraction of Fab-free HA remaining in a trimeric conformation (Figures 7G and S7H). Despite extensive trials, the intermediate stage of this structural change could not be obtained, apparently due to the rapid transformation of the HA0 from trimeric to monomeric states induced by Ab binding. These results strongly suggest that FluA-20 is indeed capable of binding the uncleaved HA0 trimer, exaggerating the trimer dynamics to almost fully dissociate the trimer *in vitro* (Figures 7F and 7G). The ability to selectively disrupt HA0 trimers on the surface of infected cells and the ability to inhibit cell-cell spread suggested that FluA-20 represents a distinct class of potent bnAbs.

DISCUSSION

Isolation of naturally occurring broad-spectrum human mAbs to IAV holds great promise for discovery of new candidate therapeutics, as well as identifying critical epitopes for rational design of structure-based broadly protective influenza vaccines. Most bnAbs with extensive heterosubtypic activities discovered to date recognize the conserved HA stem region, whereas most neutralizing Abs to the head domain react principally with a given subtype (Hong et al., 2013; Joyce et al., 2016; Julien et al., 2012; Lee et al., 2014; Thornburg et al., 2016; Whittle et al., 2011; Wu and Wilson, 2017; Xu et al., 2013; Zhu et al., 2013). Although some bnAbs that target the head domain have been isolated in recent years (Ekiert et al., 2012; Lee et al., 2012), none of them display heterosubtypic breadth comparable to that of the broadest HA stem Abs.

In this work, we report the isolation and characterization of the broadly protective Ab FluA-20 that recognizes the HA head domain from nearly all IAV HA subtypes with excellent binding affinity. The discovery of the FluA-20 epitope unexpectedly revealed a highly conserved site of vulnerability that is hidden in the HA trimer interface. Although FluA-20 does not neutralize influenza, this Ab exhibits some unique properties in that it rapidly disrupts HA trimers and inhibits the cell-to-cell spread of virus. The Ab also mediates ADCC activity *in vitro*, although this activity was not essential to the *in vivo* protective effects. FluA-20 conferred *in vivo* protection in mice against strains representing several major influenza A subtypes that are pathogenic for humans. When administered prophylactically or therapeutically, FluA-20 protected mice against challenge with diverse IAV strains. Therefore, FluA-20 is a candidate for a broad-spectrum antiviral therapeutic against various IAV infections.

It is a striking observation that FluA-20, which recognizes an epitope obscured in the HA trimer interface, is able to mediate *in vivo* protection against the viruses. Previous studies have demonstrated that the assembly of HA trimer occurs in the endoplasmic reticulum, prior to its transport to the cellular surface. Non-oligomerized HA monomers are not transported to the Golgi complex (Copeland et al., 1986; Copeland et al., 1988; Gething et al., 1986). Therefore, the HA molecules on the cellular or viral surface generally have been considered to be stable trimers, with the trimer interface regarded as inaccessible and thus not targetable by the immune response or therapeutics. The ability of FluA-20 to confer *in vivo* protection strongly suggests that HA molecules are dynamic and more heterogeneous in their conformations than we have observed previously, and that the trimer interface is partially or transiently accessible. Similar phenomenon, previously described as ''breathing,'' has been

software and represented as percentage of total well area. Each value represents mean focus area ± SD. (C) Concentration-dependent effect of focus area reduction. Each value represents the mean focus area ± SD.

(D and E) (D) and (E) correspond to the *in vivo* protective efficacy of engineered Fc mutant variants of mAb FluA-20. BALB/c mice were inoculated i.p. with 10 mg/kg of mAb on the day before challenge by the i.n. route with 1.24×10^4 FFU of A/California/04/2009 virus and monitored for 14 days. The control group was treated with mAb specific to an unrelated target. The protective efficacy of mAbs was assessed by weight change (D) and clinical score (E). The dotted line indicates the Institutional Animal Care and Use Committee (IACUC)-stipulated endpoint for humane euthanasia. Data are cumulative of 2 independent experiments and show the mean value ± SEM, using 5 to 10 mice per group. Multiple group comparisons were performed using two-way ANOVA with Tukey's post-test for (A). The results of comparison between rFluA-20 IgG1-N297A-treated (gray) and rFluA-20 IgG1-treated (blue) groups demonstrate a significant difference in weight change between these two groups (denoted with * symbol), although the N297A Fc region mutation that abrogates FcR binding had a negligible impact of on overall protection.

(F) Selected 2D class averages of H1 HA trimer (A/California/04/2009) after a 20-second incubation with FluA-20 Fab. All of the Fabs complexed HA were in monomeric form, while a few apo HA trimers were observed. All 2D class averages are shown in Figure S7B. FluA-20 Fab is blue and HA is white.

(G) Illustration showing that FluA-20 Fab (heavy chain in blue and light chain in green) dissociates native HA trimer (gray), as assessed by negative-stain EM data shown in (F) and Figure S7B.

See also Figure S7.

observed for the envelope glycoproteins from other viruses, such as West Nile virus (Dowd et al., 2011), dengue virus (Dowd and Pierson, 2018; Rey and Lok, 2018; Rey et al., 2018), and HIV (Munro et al., 2014; Munro and Mothes, 2015). Previous computational predictions also have led to speculations that mutations distant to the RBS could affect HA trimer dynamics and allosterically modify functional properties, such as receptor binding, of the HA trimer (Yoon et al., 2015). Possibly, FluA-20 influences the formation of HA trimers on the surface of infected cells and disrupts the efficient assembly of progeny viruses. The studies here provide the first high-resolution characterization of an interface epitope, demonstrating that the HA trimer could indeed feature similar "breathing" motions. We found that the dynamics of the HA trimer are more pronounced in the uncleaved HA0 form than in the cleaved HA, as assessed by HDX-MS studies. A study from Yewdell et al. (1993) reported the characterization of murine mAb Y8-10C2, the epitope of which was indicated to be present between adjacent protomers in the globular head domain by mutagenesis study. The study also implied that changes made near the fusion loop could indirectly affect the flexibility of the globular head domain and lead to resistance against Y8-10C2. The effect of trypsin-mediated cleavage on the conformational dynamics of the globular head domain in HA trimer conformation is poorly understood. HA dynamic changes also were found in the pH-activated fusion step, with the HA head interface region becoming more stabilized and the fusion peptide and surrounding HA stem residues becoming more dynamic at an intermediate pH prior to the pH of fusion (Garcia et al., 2015).

A recent study by Lee et al. (2016) reported the identification of three non-neutralizing but protective human Abs to H1 and H3 that bound to monomeric, but not trimeric, forms of HA. The 22 Å negative-stain EM models of the Fab complexes with the HA protomer indicated that these Abs bind to a region on the HA head (entirely different from the FluA-20 epitope) that is not fully accessible in the intact HA trimer. The discovery of these HA trimer interface (TI)-targeted Abs is particularly interesting in that, similar to the receptor-binding site and the stem region of HA, the trimer interface also possesses patches of highly conserved surfaces (Yusuf et al., 2013); however, these potentially vulnerable sites have not been investigated for therapeutic or vaccine development. The findings presented here could lead to more comprehensive and detailed assessments of the accessibility of the HA trimer interface and potential therapeutics or vaccines that target this hidden and conserved surface.

STAR★METHODS

Detailed methods are provided in the online version of this paper and include the following:

SUPPLEMENTAL INFORMATION

Supplemental Information can be found online at https://doi.org/10.1016/j.cell.2019.04.011.

ACKNOWLEDGMENTS

We thank Henry Tien from the robotics core in the Wilson laboratory for automated crystal screening and Wenli Yu and Yuanzi Huang in the Wilson laboratory for technical support. We thank Rachel Nargi and Rob Carnahan at Vanderbilt for help with mAb production and sequence analysis and Ryan Irving for help with mouse studies. This work was supported by grants from the NIH U19 AI117905 (to J.E.C.), R56 AI127371 (to I.A.W.), and P01 AI097092 (to A.G.-S.) and NIH contracts HHSN272201400024C (to J.E.C.) and HHSN272201400008C (to A.G.-S.). The project described was supported by CTSA award No. UL1 TR002243 from NCATS. Vanderbilt University Medical Center used the non-clinical and pre-clinical services program offered by the NIAID through Contract No. HHSN27220170041I to determine the *in vivo* activity of FluA-20 in mouse models of influenza conducted by Dr. Jonna Westover at Utah State University. The contents of this publication are solely the responsibility of the authors and do not necessarily represent the official views of NIGMS, NCATS, NIAID or NIH. X-ray diffraction data were collected at the Advanced Photon Source beamline 23ID-B (GM/CA CAT) and the Stanford Synchrotron Radiation Lightsource beamline 11-1. GM/CA@APS is funded in whole or in part with federal funds from the NCI (ACB-12002) and the NIGMS (AGM-12006). This research used resources of the Advanced Photon Source, a U.S. DOE Office of Science User Facility operated for the DOE Office of Science by Argonne National Laboratory under Contract No. DE-AC02-06CH11357. Use of the Stanford Synchrotron Radiation Lightsource, SLAC National Accelerator Laboratory, is supported by the U.S. DOE, Office of Science, Office of Basic Energy Sciences under Contract No. DE-AC02-76SF00515. The SSRL Structural Molecular Biology Program is supported by the DOE Office of Biological and Environmental Research and by the NIH, NIGMS (including P41GM103393).

AUTHOR CONTRIBUTIONS

S.B., S. Lang, I.A.W., and J.E.C. conceived and designed the research; S.B., R.B., J.A.F., and J.E.C. isolated, sequenced, and analyzed FluA-20 and its clonally related Abs; S.B., S. Lang, and I.G. performed *in vitro* profiling of FluA-20 activity; S.B., H.A.V., and S.J.K. determined the ADCC activity; S.B., M.S., P.G., I.G., and A.G.-S. performed mouse studies; S. Lang and X.Z. determined the X-ray structures; S.B. and S. Lang analyzed FluA-20/HA interactions and the epitope; S. Li performed the HDX-MS experiments; H.L.T. and A.B.W. performed and analyzed the EM experiments; S.B, S. Lang, I.A.W., and J.E.C. wrote the manuscript.

DECLARATION OF INTERESTS

J.E.C. has served as a consultant for Takeda Vaccines, Sanofi Pasteur, Pfizer, and Novavax; is on the Scientific Advisory Boards of CompuVax and Meissa Vaccines; and is Founder of IDBiologics, Inc. A.G.-S. is inventor of patents owned by the Icahn School of Medicine at Mount Sinai in the field of influenza virus vaccines and Abs. All other authors declare no conflict of interest. Vanderbilt University has applied for a patent related to the FluA-20 Ab.

Received: July 23, 2018
Revised: February 25, 2019
Accepted: April 4, 2019
Published: May 16, 2019

REFERENCES

Adams, P.D., Afonine, P.V., Bunkóczi, G., Chen, V.B., Davis, I.W., Echols, N., Headd, J.J., Hung, L.W., Kapral, G.J., Grosse-Kunstleve, R.W., et al. (2010). PHENIX: a comprehensive Python-based system for macromolecular structure solution. Acta Crystallogr. D Biol. Crystallogr. *66*, 213–221.

Aiyegbo, M.S., Eli, I.M., Spiller, B.W., Williams, D.R., Kim, R., Lee, D.E., Liu, T., Li, S., Stewart, P.L., and Crowe, J.E., Jr. (2014). Differential accessibility of a rotavirus VP6 epitope in trimers comprising type I, II, or III channels as revealed by binding of a human rotavirus VP6-specific antibody. J. Virol. *88*, 469–476.

Al-Hubeshy, Z.B., Coleman, A., Nelson, M., and Goodier, M.R. (2011). A rapid method for assessment of natural killer cell function after multiple receptor crosslinking. J. Immunol. Methods *366*, 52–59.

Alter, G., Malenfant, J.M., and Altfeld, M. (2004). CD107a as a functional marker for the identification of natural killer cell activity. J. Immunol. Methods *294*, 15–22.

Altman, M.O., Bennink, J.R., Yewdell, J.W., and Herrin, B.R. (2015). Lamprey VLRB response to influenza virus supports universal rules of immunogenicity and antigenicity. eLife *4*, 07467.

Angeletti, D., Gibbs, J.S., Angel, M., Kosik, I., Hickman, H.D., Frank, G.M., Das, S.R., Wheatley, A.K., Prabhakaran, M., Leggat, D.J., et al. (2017). Defining B cell immunodominance to viruses. Nat. Immunol. *18*, 456–463.

Arduin, E., Arora, S., Bamert, P.R., Kuiper, T., Popp, S., Geisse, S., Grau, R., Calzascia, T., Zenke, G., and Kovarik, J. (2015). Highly reduced binding to high and low affinity mouse Fc gamma receptors by L234A/L235A and N297A Fc mutations engineered into mouse IgG2a. Mol. Immunol. *63*, 456–463.

Ashkenazy, H., Abadi, S., Martz, E., Chay, O., Mayrose, I., Pupko, T., and Ben-Tal, N. (2016). ConSurf 2016: an improved methodology to estimate and visualize evolutionary conservation in macromolecules. Nucleic Acids Res. *44* (W1), W344–W350.

Bangaru, S., Nieusma, T., Kose, N., Thornburg, N.J., Finn, J.A., Kaplan, B.S., King, H.G., Singh, V., Lampley, R.M., Sapparapu, G., et al. (2016). Recognition of influenza H3N2 variant virus by human neutralizing antibodies. JCI Insight *1*, e86673.

Bangaru, S., Zhang, H., Gilchuk, I.M., Voss, T.G., Irving, R.P., Gilchuk, P., Matta, P., Zhu, X., Lang, S., Nieusma, T., et al. (2018). A multifunctional human monoclonal neutralizing antibody that targets a unique conserved epitope on influenza HA. Nat. Commun. *9*, 2669.

Bao, Y., Bolotov, P., Dernovoy, D., Kiryutin, B., Zaslavsky, L., Tatusova, T., Ostell, J., and Lipman, D. (2008). The influenza virus resource at the National Center for Biotechnology Information. J. Virol. *82*, 596–601.

Bridges, C.B., Thompson, W.W., Meltzer, M.I., Reeve, G.R., Talamonti, W.J., Cox, N.J., Lilac, H.A., Hall, H., Klimov, A., and Fukuda, K. (2000). Effectiveness and cost-benefit of influenza vaccination of healthy working adults: A randomized controlled trial. JAMA *284*, 1655–1663.

Brochet, X., Lefranc, M.P., and Giudicelli, V. (2008). IMGT/V-QUEST: the highly customized and integrated system for IG and TR standardized V-J and V-D-J sequence analysis. Nucleic Acids Res. *36*, W503–W508.

Carr, C.M., and Kim, P.S. (1993). A spring-loaded mechanism for the conformational change of influenza hemagglutinin. Cell *73*, 823–832.

Carrat, F., and Flahault, A. (2007). Influenza vaccine: the challenge of antigenic drift. Vaccine *25*, 6852–6862.

Caton, A.J., Brownlee, G.G., Yewdell, J.W., and Gerhard, W. (1982). The antigenic structure of the influenza virus A/PR/8/34 hemagglutinin (H1 subtype). Cell *31*, 417–427.

Celniker, G., Nimrod, G., Ashkenazy, H., Glaser, F., Martz, E., Mayrose, I., Pupko, T., and Ben-Tal, N. (2013). ConSurf: Using Evolutionary Data to Raise Testable Hypotheses about Protein Function. Isr. J. Chem. *53*, 199–206.

Chao, D.T., Ma, X., Li, O., Park, H., and Law, D. (2009). Functional characterization of N297A, a murine surrogate for low-Fc binding anti-human CD3 antibodies. Immunol. Invest. *38*, 76–92.

Chen, J., Lee, K.H., Steinhauer, D.A., Stevens, D.J., Skehel, J.J., and Wiley, D.C. (1998). Structure of the hemagglutinin precursor cleavage site, a determinant of influenza pathogenicity and the origin of the labile conformation. Cell *95*, 409–417.

Chen, V.B., Arendall, W.B., 3rd, Headd, J.J., Keedy, D.A., Immormino, R.M., Kapral, G.J., Murray, L.W., Richardson, J.S., and Richardson, D.C. (2010). MolProbity: all-atom structure validation for macromolecular crystallography. Acta Crystallogr. D Biol. Crystallogr. *66*, 12–21.

Copeland, C.S., Doms, R.W., Bolzau, E.M., Webster, R.G., and Helenius, A. (1986). Assembly of influenza hemagglutinin trimers and its role in intracellular transport. J. Cell Biol. *103*, 1179–1191.

Copeland, C.S., Zimmer, K.P., Wagner, K.R., Healey, G.A., Mellman, I., and Helenius, A. (1988). Folding, trimerization, and transport are sequential events in the biogenesis of influenza virus hemagglutinin. Cell *53*, 197–209.

Corti, D., Suguitan, A.L., Jr., Pinna, D., Silacci, C., Fernandez-Rodriguez, B.M., Vanzetta, F., Santos, C., Luke, C.J., Torres-Velez, F.J., Temperton, N.J., et al. (2010). Heterosubtypic neutralizing antibodies are produced by individuals immunized with a seasonal influenza vaccine. J. Clin. Invest. *120*, 1663–1673.

Corti, D., Voss, J., Gamblin, S.J., Codoni, G., Macagno, A., Jarrossay, D., Vachieri, S.G., Pinna, D., Minola, A., Vanzetta, F., et al. (2011). A neutralizing antibody selected from plasma cells that binds to group 1 and group 2 influenza A hemagglutinins. Science *333*, 850–856.

Das, S.R., Hensley, S.E., Ince, W.L., Brooke, C.B., Subba, A., Delboy, M.G., Russ, G., Gibbs, J.S., Bennink, J.R., and Yewdell, J.W. (2013). Defining influenza A virus hemagglutinin antigenic drift by sequential monoclonal antibody selection. Cell Host Microbe *13*, 314–323.

DiLillo, D.J., Tan, G.S., Palese, P., and Ravetch, J.V. (2014). Broadly neutralizing hemagglutinin stalk-specific antibodies require FcγR interactions for protection against influenza virus in vivo. Nat. Med. *20*, 143–151.

DiLillo, D.J., Palese, P., Wilson, P.C., and Ravetch, J.V. (2016). Broadly neutralizing anti-influenza antibodies require Fc receptor engagement for in vivo protection. J. Clin. Invest. *126*, 605–610.

Dowd, K.A., and Pierson, T.C. (2018). The many faces of a dynamic virion: Implications of viral breathing on flavivirus biology and immunogenicity. Annu. Rev. Virol. *5*, 185–207.

Dowd, K.A., Jost, C.A., Durbin, A.P., Whitehead, S.S., and Pierson, T.C. (2011). A dynamic landscape for antibody binding modulates antibody-mediated neutralization of West Nile virus. PLoS Pathog. *7*, e1002111.

Dreyfus, C., Laursen, N.S., Kwaks, T., Zuijdgeest, D., Khayat, R., Ekiert, D.C., Lee, J.H., Metlagel, Z., Bujny, M.V., Jongeneelen, M., et al. (2012). Highly conserved protective epitopes on influenza B viruses. Science *337*, 1343–1348.

Dreyfus, C., Ekiert, D.C., and Wilson, I.A. (2013). Structure of a classical broadly neutralizing stem antibody in complex with a pandemic H2 influenza virus hemagglutinin. J. Virol. *87*, 7149–7154.

Edgar, R.C. (2004). MUSCLE: multiple sequence alignment with high accuracy and high throughput. Nucleic Acids Res. *32*, 1792–1797.

Ekiert, D.C., Bhabha, G., Elsliger, M.A., Friesen, R.H., Jongeneelen, M., Throsby, M., Goudsmit, J., and Wilson, I.A. (2009). Antibody recognition of a highly conserved influenza virus epitope. Science *324*, 246–251.

Ekiert, D.C., Friesen, R.H., Bhabha, G., Kwaks, T., Jongeneelen, M., Yu, W., Ophorst, C., Cox, F., Korse, H.J., Brandenburg, B., et al. (2011). A highly conserved neutralizing epitope on group 2 influenza A viruses. Science *333*, 843–850.

Ekiert, D.C., Kashyap, A.K., Steel, J., Rubrum, A., Bhabha, G., Khayat, R., Lee, J.H., Dillon, M.A., O'Neil, R.E., Faynboym, A.M., et al. (2012). Cross-neutralization of influenza A viruses mediated by a single antibody loop. Nature *489*, 526–532.

Emsley, P., and Cowtan, K. (2004). Coot: model-building tools for molecular graphics. Acta Crystallogr. D Biol. Crystallogr. *60*, 2126–2132.

Freidl, G.S., Meijer, A., de Bruin, E., de Nardi, M., Munoz, O., Capua, I., Breed, A.C., Harris, K., Hill, A., Kosmider, R., et al.; FLURISK Consortium (2014). Influenza at the animal-human interface: a review of the literature for virological evidence of human infection with swine or avian influenza viruses other than A(H5N1). Euro Surveill. *19*, 20793.

Friesen, R.H., Lee, P.S., Stoop, E.J., Hoffman, R.M., Ekiert, D.C., Bhabha, G., Yu, W., Juraszek, J., Koudstaal, W., Jongeneelen, M., et al. (2014). A common solution to group 2 influenza virus neutralization. Proc. Natl. Acad. Sci. USA *111*, 445–450.

Garces, F., Lee, J.H., de Val, N., de la Pena, A.T., Kong, L., Puchades, C., Hua, Y., Stanfield, R.L., Burton, D.R., Moore, J.P., et al. (2015). Affinity maturation of a potent family of HIV antibodies is primarily focused on accommodating or avoiding glycans. Immunity *43*, 1053–1063.

Garcia, N.K., Guttman, M., Ebner, J.L., and Lee, K.K. (2015). Dynamic changes during acid-induced activation of influenza hemagglutinin. Structure *23*, 665–676.

Gerhard, W., Yewdell, J., Frankel, M.E., and Webster, R. (1981). Antigenic structure of influenza virus haemagglutinin defined by hybridoma antibodies. Nature *290*, 713–717.

Gething, M.J., McCammon, K., and Sambrook, J. (1986). Expression of wild-type and mutant forms of influenza hemagglutinin: the role of folding in intracellular transport. Cell *46*, 939–950.

Giudicelli, V., and Lefranc, M.P. (2011). IMGT/junctionanalysis: IMGT standardized analysis of the V-J and V-D-J junctions of the rearranged immunoglobulins (IG) and T cell receptors (TR). Cold Spring Harb. Protoc. *2011*, 716–725.

Hamuro, Y., Anand, G.S., Kim, J.S., Juliano, C., Stranz, D.D., Taylor, S.S., and Woods, V.L., Jr. (2004). Mapping intersubunit interactions of the regulatory subunit (RIalpha) in the type I holoenzyme of protein kinase A by amide hydrogen/deuterium exchange mass spectrometry (DXMS). J. Mol. Biol. *340*, 1185–1196.

He, W., Mullarkey, C.E., Duty, J.A., Moran, T.M., Palese, P., and Miller, M.S. (2015). Broadly neutralizing anti-influenza virus antibodies: enhancement of neutralizing potency in polyclonal mixtures and IgA backbones. J. Virol. *89*, 3610–3618.

Hezareh, M., Hessell, A.J., Jensen, R.C., van de Winkel, J.G., and Parren, P.W. (2001). Effector function activities of a panel of mutants of a broadly neutralizing antibody against human immunodeficiency virus type 1. J. Virol. *75*, 12161–12168.

Hong, M., Lee, P.S., Hoffman, R.M., Zhu, X., Krause, J.C., Laursen, N.S., Yoon, S.I., Song, L., Tussey, L., Crowe, J.E., Jr., et al. (2013). Antibody recognition of the pandemic H1N1 Influenza virus hemagglutinin receptor binding site. J. Virol. *87*, 12471–12480.

Hsu, S., Kim, Y., Li, S., Durrant, E.S., Pace, R.M., Woods, V.L., Jr., and Gentry, M.S. (2009). Structural insights into glucan phosphatase dynamics using amide hydrogen-deuterium exchange mass spectrometry. Biochemistry *48*, 9891–9902.

Irimia, A., Sarkar, A., Stanfield, R.L., and Wilson, I.A. (2016). Crystallographic identification of lipid as an integral component of the epitope of HIV broadly neutralizing antibody 4E10. Immunity *44*, 21–31.

Jegaskanda, S., Job, E.R., Kramski, M., Laurie, K., Isitman, G., de Rose, R., Winnall, W.R., Stratov, I., Brooks, A.G., Reading, P.C., and Kent, S.J. (2013). Cross-reactive influenza-specific antibody-dependent cellular cytotoxicity antibodies in the absence of neutralizing antibodies. J. Immunol. *190*, 1837–1848.

Joyce, M.G., Wheatley, A.K., Thomas, P.V., Chuang, G.Y., Soto, C., Bailer, R.T., Druz, A., Georgiev, I.S., Gillespie, R.A., Kanekiyo, M., et al.; NISC Comparative Sequencing Program (2016). Vaccine-induced antibodies that neutralize group 1 and group 2 influenza A viruses. Cell *166*, 609–623.

Julien, J.P., Lee, P.S., and Wilson, I.A. (2012). Structural insights into key sites of vulnerability on HIV-1 Env and influenza HA. Immunol. Rev. *250*, 180–198.

Kallewaard, N.L., Corti, D., Collins, P.J., Neu, U., McAuliffe, J.M., Benjamin, E., Wachter-Rosati, L., Palmer-Hill, F.J., Yuan, A.Q., Walker, P.A., et al. (2016). Structure and function analysis of an antibody recognizing all influenza A subtypes. Cell *166*, 596–608.

Kashyap, A.K., Steel, J., Oner, A.F., Dillon, M.A., Swale, R.E., Wall, K.M., Perry, K.J., Faynboym, A., Ilhan, M., Horowitz, M., et al. (2008). Combinatorial antibody libraries from survivors of the Turkish H5N1 avian influenza outbreak reveal virus neutralization strategies. Proc. Natl. Acad. Sci. USA *105*, 5986–5991.

Kashyap, A.K., Steel, J., Rubrum, A., Estelles, A., Briante, R., Ilyushina, N.A., Xu, L., Swale, R.E., Faynboym, A.M., Foreman, P.K., et al. (2010). Protection from the 2009 H1N1 pandemic influenza by an antibody from combinatorial survivor-based libraries. PLoS Pathog. *6*, e1000990.

Kristensen, A.B., Lay, W.N., Ana-Sosa-Batiz, F., Vanderven, H.A., Madhavi, V., Laurie, K.L., Carolan, L., Wines, B.D., Hogarth, M., Wheatley, A.K., and Kent,

S.J. (2016). Antibody responses with Fc-mediated functions after vaccination of HIV-infected subjects with trivalent influenza vaccine. J. Virol. *90*, 5724–5734.

Lander, G.C., Stagg, S.M., Voss, N.R., Cheng, A., Fellmann, D., Pulokas, J., Yoshioka, C., Irving, C., Mulder, A., Lau, P.W., et al. (2009). Appion: an integrated, database-driven pipeline to facilitate EM image processing. J. Struct. Biol. *166*, 95–102.

Lang, S., Xie, J., Zhu, X., Wu, N.C., Lerner, R.A., and Wilson, I.A. (2017). Antibody 27F3 broadly targets influenza A group 1 and 2 hemagglutinins through a further variation in VH1-69 antibody orientation on the HA stem. Cell Rep. *20*, 2935–2943.

Laursen, N.S., and Wilson, I.A. (2013). Broadly neutralizing antibodies against influenza viruses. Antiviral Res. *98*, 476–483.

Lee, P.S., Yoshida, R., Ekiert, D.C., Sakai, N., Suzuki, Y., Takada, A., and Wilson, I.A. (2012). Heterosubtypic antibody recognition of the influenza virus hemagglutinin receptor binding site enhanced by avidity. Proc. Natl. Acad. Sci. USA *109*, 17040–17045.

Lee, P.S., Ohshima, N., Stanfield, R.L., Yu, W., Iba, Y., Okuno, Y., Kurosawa, Y., and Wilson, I.A. (2014). Receptor mimicry by antibody F045-092 facilitates universal binding to the H3 subtype of influenza virus. Nat. Commun. *5*, 3614.

Lee, J., Boutz, D.R., Chromikova, V., Joyce, M.G., Vollmers, C., Leung, K., Horton, A.P., DeKosky, B.J., Lee, C.H., Lavinder, J.J., et al. (2016). Molecular-level analysis of the serum antibody repertoire in young adults before and after seasonal influenza vaccination. Nat. Med. *22*, 1456–1464.

Li, S., Tsalkova, T., White, M.A., Mei, F.C., Liu, T., Wang, D., Woods, V.L., Jr., and Cheng, X. (2011). Mechanism of intracellular cAMP sensor Epac2 activation: cAMP-induced conformational changes identified by amide hydrogen/deuterium exchange mass spectrometry (DXMS). J. Biol. Chem. *286*, 17889–17897.

Lu, W.D., Liu, T., Li, S., Woods, V.L., Jr., and Hook, V. (2012). The prohormone proenkephalin possesses differential conformational features of subdomains revealed by rapid H-D exchange mass spectrometry. Protein Sci. *21*, 178–187.

Marsh, J.J., Guan, H.S., Li, S., Chiles, P.G., Tran, D., and Morris, T.A. (2013). Structural insights into fibrinogen dynamics using amide hydrogen/deuterium exchange mass spectrometry. Biochemistry *52*, 5491–5502.

McCoy, A.J., Grosse-Kunstleve, R.W., Adams, P.D., Winn, M.D., Storoni, L.C., and Read, R.J. (2007). Phaser crystallographic software. J. Appl. Cryst. *40*, 658–674.

McLean, G.R., Nakouzi, A., Casadevall, A., and Green, N.S. (2000). Human and murine immunoglobulin expression vector cassettes. Mol Immunol. *37*, 837–845.

Morgan, A., Jones, N.D., Nesbitt, A.M., Chaplin, L., Bodmer, M.W., and Emtage, J.S. (1995). The N-terminal end of the CH2 domain of chimeric human IgG1 anti-HLA-DR is necessary for C1q, Fc gamma RI and Fc gamma RIII binding. Immunology *86*, 319–324.

Munro, J.B., and Mothes, W. (2015). Structure and dynamics of the native HIV-1 env trimer. J. Virol. *89*, 5752–5755.

Munro, J.B., Gorman, J., Ma, X., Zhou, Z., Arthos, J., Burton, D.R., Koff, W.C., Courter, J.R., Smith, A.B., 3rd, Kwong, P.D., et al. (2014). Conformational dynamics of single HIV-1 envelope trimers on the surface of native virions. Science *346*, 759–763.

Neumann, G., and Kawaoka, Y. (2015). Transmission of influenza A viruses. Virology *479-480*, 234–246.

Nobusawa, E., Aoyama, T., Kato, H., Suzuki, Y., Tateno, Y., and Nakajima, K. (1991). Comparison of complete amino acid sequences and receptor-binding properties among 13 serotypes of hemagglutinins of influenza A viruses. Virology *182*, 475–485.

Nordin, J., Mullooly, J., Poblete, S., Strikas, R., Petrucci, R., Wei, F., Rush, B., Safirstein, B., Wheeler, D., and Nichol, K.L. (2001). Influenza vaccine effectiveness in preventing hospitalizations and deaths in persons 65 years or older in Minnesota, New York, and Oregon: data from 3 health plans. J. Infect. Dis. *184*, 665–670.

Ogura, T., Iwasaki, K., and Sato, C. (2003). Topology representing network enables highly accurate classification of protein images taken by cryo electron-microscope without masking. J. Struct. Biol. *143*, 185–200.

Okuno, Y., Isegawa, Y., Sasao, F., and Ueda, S. (1993). A common neutralizing epitope conserved between the hemagglutinins of influenza A virus H1 and H2 strains. J. Virol. *67*, 2552–2558.

Potter, C.S., Chu, H., Frey, B., Green, C., Kisseberth, N., Madden, T.J., Miller, K.L., Nahrstedt, K., Pulokas, J., Reilein, A., et al. (1999). Leginon: a system for fully automated acquisition of 1000 electron micrographs a day. Ultramicroscopy *77*, 153–161.

Rey, F.A., and Lok, S.M. (2018). Common features of enveloped viruses and implications for immunogen design for next-generation vaccines. Cell *172*, 1319–1334.

Rey, F.A., Stiasny, K., Vaney, M.C., Dellarole, M., and Heinz, F.X. (2018). The bright and the dark side of human antibody responses to flaviviruses: lessons for vaccine design. EMBO Rep. *19*, 206–224.

Rice, P., Longden, I., and Bleasby, A. (2000). EMBOSS: the european molecular biology open software suite. Trends Genet. *16*, 276–277.

Russell, R.J., Gamblin, S.J., Haire, L.F., Stevens, D.J., Xiao, B., Ha, Y., and Skehel, J.J. (2004). H1 and H7 influenza haemagglutinin structures extend a structural classification of haemagglutinin subtypes. Virology *325*, 287–296.

Schmidt, A.G., Therkelsen, M.D., Stewart, S., Kepler, T.B., Liao, H.X., Moody, M.A., Haynes, B.F., and Harrison, S.C. (2015). Viral receptor-binding site antibodies with diverse germline origins. Cell *161*, 1026–1034.

Skubák, P., Murshudov, G.N., and Pannu, N.S. (2004). Direct incorporation of experimental phase information in model refinement. Acta Crystallogr. D Biol. Crystallogr. *60*, 2196–2201.

Smirnov, Y.A., Lipatov, A.S., Gitelman, A.K., Okuno, Y., Van Beek, R., Osterhaus, A.D., and Claas, E.C. (1999). An epitope shared by the hemagglutinins of H1, H2, H5, and H6 subtypes of influenza A virus. Acta Virol. *43*, 237–244.

Smith, S.A., Zhou, Y., Olivarez, N.P., Broadwater, A.H., de Silva, A.M., and Crowe, J.E., Jr. (2012). Persistence of circulating memory B cell clones with potential for dengue virus disease enhancement for decades following infection. J. Virol. *86*, 2665–2675.

Steinhauer, D.A. (1999). Role of hemagglutinin cleavage for the pathogenicity of influenza virus. Virology *258*, 1–20.

Thornburg, N.J., Zhang, H., Bangaru, S., Sapparapu, G., Kose, N., Lampley, R.M., Bombardi, R.G., Yu, Y., Graham, S., Branchizio, A., et al. (2016). H7N9 influenza virus neutralizing antibodies that possess few somatic mutations. J. Clin. Invest. *126*, 1482–1494.

Tong, S., Zhu, X., Li, Y., Shi, M., Zhang, J., Bourgeois, M., Yang, H., Chen, X., Recuenco, S., Gomez, J., et al. (2013). New world bats harbor diverse influenza A viruses. PLoS Pathog. *9*, e1003657.

van Dongen, J.J., Langerak, A.W., Brüggemann, M., Evans, P.A., Hummel, M., Lavender, F.L., Delabesse, E., Davi, F., Schuuring, E., García-Sanz, R., et al. (2003). Design and standardization of PCR primers and protocols for detection of clonal immunoglobulin and T-cell receptor gene recombinations in suspect lymphoproliferations: report of the BIOMED-2 Concerted Action BMH4-CT98-3936. Leukemia *17*, 2257–2317.

Voss, N.R., Yoshioka, C.K., Radermacher, M., Potter, C.S., and Carragher, B. (2009). DoG Picker and TiltPicker: software tools to facilitate particle selection in single particle electron microscopy. J. Struct. Biol. *166*, 205–213.

Weis, W., Brown, J.H., Cusack, S., Paulson, J.C., Skehel, J.J., and Wiley, D.C. (1988). Structure of the influenza virus haemagglutinin complexed with its receptor, sialic acid. Nature *333*, 426–431.

Whittle, J.R.R., Zhang, R., Khurana, S., King, L.R., Manischewitz, J., Golding, H., Dormitzer, P.R., Haynes, B.F., Walter, E.B., Moody, M.A., et al. (2011). Broadly neutralizing human antibody that recognizes the receptor-binding pocket of influenza virus hemagglutinin. Proc. Natl. Acad. Sci. USA *108*, 14216–14221.

Wilson, I.A., Skehel, J.J., and Wiley, D.C. (1981). Structure of the haemagglutinin membrane glycoprotein of influenza virus at 3 Å resolution. Nature *289*, 366–373.

Wines, B.D., Vanderven, H.A., Esparon, S.E., Kristensen, A.B., Kent, S.J., and Hogarth, P.M. (2016). Dimeric FcγR ectodomains as probes of the Fc receptor function of anti-influenza virus IgG. J. Immunol. *197*, 1507–1516.

Wu, N.C., and Wilson, I.A. (2017). A perspective on the structural and functional constraints for immune evasion: insights from influenza virus. J. Mol. Biol. *429*, 2694–2709.

Xu, R., Krause, J.C., McBride, R., Paulson, J.C., Crowe, J.E., Jr., and Wilson, I.A. (2013). A recurring motif for antibody recognition of the receptor-binding site of influenza hemagglutinin. Nat. Struct. Mol. Biol. *20*, 363–370.

Yewdell, J.W., Taylor, A., Yellen, A., Caton, A., Gerhard, W., and Bächi, T. (1993). Mutations in or near the fusion peptide of the influenza virus hemagglutinin affect an antigenic site in the globular region. J. Virol. *67*, 933–942.

Yoon, S.W., Chen, N., Ducatez, M.F., McBride, R., Barman, S., Fabrizio, T.P., Webster, R.G., Haliloglu, T., Paulson, J.C., Russell, C.J., et al. (2015). Changes to the dynamic nature of hemagglutinin and the emergence of the 2009 pandemic H1N1 influenza virus. Sci. Rep. *5*, 12828.

Yoshida, R., Igarashi, M., Ozaki, H., Kishida, N., Tomabechi, D., Kida, H., Ito, K., and Takada, A. (2009). Cross-protective potential of a novel monoclonal antibody directed against antigenic site B of the hemagglutinin of influenza A viruses. PLoS Pathog. *5*, e1000350.

Yusuf, M., Konc, J., Sy Bing, C., Trykowska Konc, J., Ahmad Khairudin, N.B., Janezic, D., and Wahab, H.A. (2013). Structurally conserved binding sites of hemagglutinin as targets for influenza drug and vaccine development. J. Chem. Inf. Model. *53*, 2423–2436.

Zhang, Z., and Smith, D.L. (1993). Determination of amide hydrogen exchange by mass spectrometry: a new tool for protein structure elucidation. Protein Sci. *2*, 522–531.

Zhu, X., Guo, Y.H., Jiang, T., Wang, Y.D., Chan, K.H., Li, X.F., Yu, W., McBride, R., Paulson, J.C., Yuen, K.Y., et al. (2013). A unique and conserved neutralization epitope in H5N1 influenza viruses identified by an antibody against the A/Goose/Guangdong/1/96 hemagglutinin. J. Virol. *87*, 12619–12635.

STAR★METHODS

KEY RESOURCES TABLE

REAGENT or RESOURCE	SOURCE	IDENTIFIER
Antibodies		
FluA-20 (hybridoma-produced IgG)	This study	N/A
Anti-human IgG alkaline phosphatase conjugate	Meridian Life Science	Cat# W99008A; RRID: AB_205090
Horseradish peroxidase-conjugated sheep-derived anti-mouse serum	GE Healthcare UK	Cat# NA-931; RRID: AB_772210
Mouse anti-human CD107a allophycocyanin-H7 antibody (clone H4A3)	BD Biosciences	Cat# 561343; RRID: AB_10644020
Anti-human CD3 PerCP (clone SP34-2)	BD Biosciences	Cat# 552851; RRID: AB_394492
Anti-human CD56 allophycocyanin (clone B159)	BD Biosciences	Cat# 555518; RRID: AB_398601
Anti-human IFNγ AF700 (clone B27)	BD Biosciences	Cat# 561024; RRID: AB_2033976
Mouse anti-NP antibody	BEI Resources	Cat# NR 4282; RRID: AB_2713892
Goat anti-human IgG PE antibody	Southern Biotech	Cat# 2040-09; RRID: AB_2795648
Biological Samples		
PBMCs from influenza vaccine	This paper	N/A
Chemicals, Peptides, and Recombinant Proteins		
Polyethylenimine (PEI) transfection reagent	Polysciences	Cat# 23966
HisTrap TALON FF crude columns	GE Healthcare Life Sciences	Cat# 28953766
CpG10103 (ODN 2006)	Invivogen	Cat# tlrl-2006
Cyclosporin A	Sigma-Aldrich	Cat# C1832
Chk2 inhibitor	Sigma-Aldrich	Cat# C3742
TPCK-treated trypsin	Sigma-Aldrich	Cat# 4370285
TrueBlue substrate	KPL-Seracare	Cat# 5510-0031
1X kinetic buffer	FortéBio	Cat# 18-5032
Ni-NTA Superflow	Qiagen	Cat# 30410
Superdex75 column	GE Healthcare	Cat# 29148721
FluoSpheres NeutrAvidin-Labeled Microspheres	ThermoFisher	Cat# F-8776
EZ-Link Sulfo-NHS-LC-LC-Biotin	ThermoFisher	Cat# 21338
1-Step Ultra TMB-ELISA	ThermoFisher	Cat# 34029
Freestyle 293 expression medium	ThermoFisher	Cat# 12338002
ExpiCHO Expression Medium	ThermoFisher	Cat# A2910001
Fetal Bovine Serum, ultra-low IgG	ThermoFisher	Cat# 16250078
ClonaCell-HY Medium E	Stem Cell Technologies	Cat# 03805
ClonaCell-HY Medium A	Stem Cell Technologies	Cat# 03801
GIBCO Hybridoma-SFM serum free medium	Invitrogen	Cat# 12045084
Dulbecco's Modified Eagle Medium (Gibco DMEM)	Invitrogen	Cat# 11965
NEBuilder HiFi DNA Assembly master mix	New England BioLabs	Cat# E2621S
Pierce High Sensitivity Streptavidin-HRP	ThermoFisher Scientific	Cat# 21130
brefeldin A	Sigma-Aldrich	Cat# B6542
monensin (BD GolgiStop)	BD Biosciences	Cat# 554724
Critical Commercial Assays		
OneStep SuperScript III with Platinum Taq High Fidelity kit	Invitrogen	Cat# 11304011
Illumina TruSeq Library Preparation Kit	Illumina	Cat# FC-121-3001
RNeasy Mini kit	Qiagen	Cat# 74106

(*Continued on next page*)

Continued

REAGENT or RESOURCE	SOURCE	IDENTIFIER
PrimeScript One Step RT-PCR kit	Clontech	Cat# RR055A
Agencourt AMPure XP magnetic beads	Beckman Coulter	Cat# A63881
Bac-to-Bac Baculovirus Expression System	Invitrogen	Cat# 10359016
Streptavidin-coated biosensor tips	FortéBio	Cat# 18-5021
Anti-human CH1 biosensor tips	FortéBio	Cat# 18-5127
Quickchange Lightning Multi-Site Mutagenesis kit	Agilent	Cat# 210515-5
EasySep human NK cell enrichment kit	STEMCELL Technologies	Cat# 19055
Deposited Data		
Apo FluA-20 Fab	This paper	PDB: 6OBZ
FluA-20 in complex with H1 head domain	This paper	PDB: 6OC3
FluA-20 in complex with H3 head domain	This paper	PDB: 6OCB
Experimental Models: Cell Lines		
Mouse-human HMAA 2.5 myeloma cell line	L. Cavacini	N/A
Hamster: ExpiCHO-S	ThermoFisher Scientific	Cat# A29127
Human: FreeStyle 293F	ThermoFisher Scientific	Cat# R79007
FluA-20 hybridoma clone	This study	N/A
Experimental Models: Organisms/Strains		
Mouse: BALB/cJ	The Jackson Laboratory	N/A
Mouse: DBA/2J	The Jackson Laboratory	N/A
Recombinant DNA		
Plasmid: pML-huCG1	McLean et al., 2000	N/A
Plasmid: pcDNA3.1(+) mammalian expression vector	Invitrogen	Cat# V79020
Software and Algorithms		
GraphPad Prism 8.0	GraphPad Software, Inc.	https://www.graphpad.com
FlowJo version 10	Tree Star	https://www.flowjo.com/solutions/flowjo/ downloads
ImMunoGeneTics database	Giudicelli and Lefranc, 2011	http://www.imgt.org/
Phaser	McCoy et al., 2007	http://www.ccp4.ac.uk/html/phaser.html
Refmac	Skubák et al., 2004	http://www.ccp4.ac.uk/dist/html/refmac5.html
Phenix	Adams et al., 2010	https://www.phenix-online.org/
Coot	Emsley and Cowtan, 2004	https://www2.mrc-lmb.cam.ac.uk/personal/pemsley/coot/
MolProbity	Chen et al., 2010	https://www.phenix-online.org/documentation/tutorials/molprobity.html
PDBePISA	Open source	www.ebi.ac.uk/pdbe/pisa/
Proteome Discoverer software	Thermo Finnigan	N/A
DXMS Explorer	Sierra Analytics, Modesto, CA	N/A
Influenza Virus Resource	Bao et al., 2008	NCBI database
MUSCLE	Edgar, 2004	N/A
ConSurf server	Ashkenazy et al., 2016; Celniker et al., 2013	N/A
Agilent QuikChange Primer Design program	Agilent Technologies	N/A
DoGpicker	Voss et al., 2009	http://emg.nysbc.org/redmine/projects/software/wiki/DoGpicker
Appion	Lander et al., 2009	http://emg.nysbc.org/redmine/projects/appion/wiki/Appion_Home
Pymol	Schrödinger	https://www.pymol.org/

(*Continued on next page*)

Continued

REAGENT or RESOURCE	SOURCE	IDENTIFIER
Other		
ECM 2001 electro cell manipulator	BTX	N/A
Octet Red instrument	FortéBio	N/A
Orbitrap Elite mass spectrometer	Thermo-Fisher Scientific	N/A
LSRFortessa flow cytometer	BD Biosciences	N/A
LSR-2 cytometer	BD Biosciences	N/A
ECM 2001 Electro Cell Manipulator	BTX	N/A
ÄKTA pure chromatography system	GE Healthcare	N/A
Synergy H1 microplate reader	BioTek	N/A
Synergy 2 microplate reader	BioTek	N/A
EL406 washer dispenser	BioTek	N/A
Biostack microplate stacker	BioTek	N/A
HiTrap Protein G High Performance	GE Healthcare	Cat# 17-0404-01
CrystalMation system	Rigaku	N/A
BioXP 3200 System	Synthetic Genomics	N/A
Immunospot S5 Analyzer	CTL	N/A
OrbiTrap Elite Mass Spectrometer	Thermo Fisher Scientific	N/A
Spirit electron microscope with TemCam F416 4k × 4k CCD	Tecnai	N/A
HiTrap MabSelect SuRe 5 mL column	GE Healthcare	Cat# 11-0034-93
Zeba Spin Desalting Columns, 7K MWCO, 0.5 mL	ThermoFisher	Cat# PI-89883
Superdex 200 Increase 10/300 GL column	GE Healthcare	N/A

CONTACT FOR REAGENT AND RESOURCE SHARING

Further information and requests for resources and reagents should be directed to and will be fulfilled by the Lead Contact, James E. Crowe, Jr. (james.crowe@vanderbilt.edu).

METHOD DETAILS

Expression of Soluble HA Proteins

Sequences encoding the HA genes of interest were optimized for mammalian cell expression, and cDNAs were synthesized (Genscript) as soluble trimeric constructs as described previously (Bangaru et al., 2016). HA protein was expressed by transient transfection of 293F cells with polyethylenimine (PEI) transfection reagent and grown in expression medium (Freestyle 293 Expression Medium; Invitrogen, 12338). Cell supernatants were harvested after 7 days, filtered sterilized with a 0.4 μm filter and recombinant protein purified with HisTrap TALON FF crude columns (GE Healthcare Life Sciences).

PBMC Isolation and Hybridoma Generation

The study was approved by the Vanderbilt University Medical Center Institutional Review Board. Peripheral blood was collected from a healthy donor with prior history of many seasonal influenza vaccinations experimental H5N1 subunit vaccinations after written informed consent. PBMCs from the donor were isolated by density gradient separation on Ficoll, cryopreserved and stored in the vapor phase of liquid nitrogen until use. Generation of human hybridoma cell lines secreting human mAbs was performed as described previously (Smith et al., 2012). Briefly, human B cells in the PBMC suspension were immortalized by transformation with EBV in the presence of CpG10103, cyclosporin A, and a Chk2 inhibitor and plated in 384-well culture plates. On day 8, the supernatants from transformed B cells were used to screen for the presence of heterosubtypic Abs that bound broadly to HA antigens from H1, H3, H7 or H9 subtypes using a capture ELISA. The recombinant HA antigens used for screening were based on the sequence of HAs from the following influenza strains: H1 A/California/04/2009, H1 A/Texas/36/1991, H3 A/Hong Kong/1/1968, H3 A/Victoria/3/1975, H7 A/Shanghai/2/2013, H7 A/Netherlands/219/2003 or H9 A/Hong Kong/1073/99. Cells from the wells containing B cells secreting heterosubtypic HA-reactive Abs were fused with HMMA2.5 myeloma cells using a BTX ECM 2001 electro cell manipulator. After fusion, human hybridomas were selected in medium with HAT solution containing ouabain. The hybridomas were cloned by flow cytometric sorting of single cells into 384-well plates and then expanded in culture. Particular clones for

downstream studies were selected by choosing the clone for each independently derived hybridoma line that exhibited the highest level of IgG secretion.

Production of IgG for mAb FluA-20 from Hybridoma Cells

The selected cloned cell line secreting mAb FluA-20 was grown initially in hybridoma growth medium (ClonaCell-HY medium E from STEMCELL Technologies, 03805) and then switched to serum-free medium (GIBCO Hybridoma-SFM, Invitrogen, 12045084) for Ab expression and purification. IgG from the hybridoma cell line supernatants was purified by affinity chromatography using protein G columns (GE Life Sciences, Protein G HP Columns). Purified FluA-20 IgG generated from hybridomas was used for all EC_{50} and IC_{50} studies, competition-binding studies, HDX-MS studies, and ADCC assays and mouse studies.

Next-Generation DNA Sequence Analysis of Expressed Ab Variable Genes

Total RNA was extracted from 10 million PBMCs. A one-step RT-PCR was performed for 25 cycles using heavy-chain BIOMED-2 variable Ab gene-specific primers as previously described (Bangaru et al., 2016; Thornburg et al., 2016) (van Dongen et al., 2003) and the OneStep SuperScript III with Platinum Taq High Fidelity kit (Invitrogen, 11304011). The Illumina-specific adapters were added using the Illumina TruSeq Library Preparation Kit (Illumina, FC-121-3001) according to the manufacturer's recommendations. The final amplicon libraries were sequenced on an Illumina MiSeq instrument using the MiSeq PE-300 v3 reagent kit (Illumina, MS-102-3001). Sequence analysis was performed using IG-BLAST v1.4, and results were parsed to MongoDB for further study.

Identifying Clonally Related Sequences

From a database of annotated Ab sequences obtained from this donor, we queried HCDR3s in sequences encoded by both of the inferred germline genes for FluA-20 (*V_H4-61* and *J_H4*). These HCDR3 sequences were pairwise aligned to the HCDR3 of FluA-20 using a PAM30 matrix, with penalties for gap opening and gap extension of -14 and -3, respectively. HCDR3 sequences with a Hamming distance of ≤ 3 to FluA-20 were selected as siblings and the "full length" nucleotide and amino acid sequence was queried from our database for further analysis.

Visualizing Clonally Related Sequences

A network graph was built from the aligned, full-length sequences queried as described above. Identical sequences were clustered into single nodes, and edges were drawn between two nodes if their Hamming distance was the lowest compared to all other nodes. Nodes denoting the inferred common ancestor and the germline *V_H4-61*/*J_H4* sequence were added manually. This network was visualized using Cytoscape and manually adjusted for visual clarity (to prevent nodes from overlapping edges to which they are not connected, and to shorten distances between nodes that are closely related).

Characterization of Ab Isotype, Subclass, and Variable Genes

The isotype and subclass of secreted Abs were determined by ELISA. Ab heavy and light chain variable region genes were sequenced from antigen-specific hybridoma lines that had been cloned biologically using flow cytometric single cell sorting. Briefly, total RNA was extracted using the RNeasy Mini kit (Qiagen, 74106) and reverse-transcriptase PCR (RT-PCR) amplification of the Ab gene cDNAs was performed using the PrimeScript One Step RT-PCR kit (Clontech, RR055A) according to the manufacturer's protocols with gene-specific primers as previously described (Thornburg et al., 2016). PCR products were purified using Agencourt AMPure XP magnetic beads (Beckman Coulter) and sequenced directly using an ABI3700 automated DNA sequencer without cloning. The identities of gene segments and mutations from germlines were determined by alignment using ImMunoGeneTics database (Brochet et al., 2008; Giudicelli and Lefranc, 2011).

Determination of Half Maximal Effective Concentration (EC_{50}) for Binding

To determine EC_{50} concentrations for binding, we performed ELISA using 384-well plates that were coated overnight at 2 μg/mL with the recombinant HA protein of interest. The plates then were blocked with 50 μL of 5% non-fat dry milk, 2% goat serum and 0.1% Tween-20 in PBS for 1 h at RT. The plates were washed and three-fold dilutions of the mAb starting from 10 μg/mL were added to the wells and incubated for 1 h. The plates were washed and 25 μL of 1:4,000 dilution of anti-human IgG alkaline phosphatase conjugate (Meridian Life Science, W99008A) was added. After a final wash, 25 μL of phosphatase substrate solution (1 mg/mL p-nitrophenol phosphate in 1 M Tris aminomethane) was added to the plates, incubated for 20 min and the optical density values were measured at 405 nm wavelength on a BioTek plate reader. The plates were washed 3 times between each step with PBS containing 0.1% Tween-20. Each dilution was performed in quadruplicate, and the EC_{50} values were calculated in Prism software (GraphPad) using non-linear regression analysis. The experiment was conducted twice independently.

Prophylaxis Studies with Sublethal Challenge and Therapeutic Studies with Lethal Challenge in Mice

Female BALB/c mice aged 6 to 8 weeks were obtained from Charles River Laboratories, Wilmington, MA, and housed under specified pathogen-free conditions with food and water *ad libitum*. For the prophylaxis studies, experimental groups of 8 mice were given i.p.

with 10 mg/kg of either FluA-20 or a similarly prepared control human Ab to an unrelated target (a mAb to methicillin-resistant *Staphylococcus aureus*; MRSA). They were challenged 24 h later with a sublethal dose (0.1 LD_{50}) of either H1N1 A/Netherlands/602/2009 or H3N2 A/X-31 (6:2 PR8 backbone) or H5N1 A/barn swallow/Hong Kong/D10-1161/2010 (7:1 PR8 backbone) or H7N9 A/Shanghai/1/2013 (6:2 PR8 backbone). Challenge under mild ketamine/xylazine anesthesia was by intranasal administration of 50 μl virus preparation diluted in PBS. Body weight change after virus challenge was used to assess protection. Mice (n = 5) were weighed every day for 14 days post-challenge. The significance in weight loss between FluA-20 and the control group was calculated for each day using 2-way ANOVA with Tukey's multiple comparisons test and displayed on the graph as *$p < 0.05$, **$p < 0.01$, and ***$p < 0.001$.

For the treatment studies, experimental groups of five mice were challenged with 1.2 LD_{50} of H3N2, H5N1 or H7N9 viruses on PR8 backbone—a dose that resulted in 40 to 100% lethality in mock-treated animals. Mice were given 10 mg/kg of FluA-20 or irrelevant Ab (MRSA) via the intraperitoneal route on days 1, 2 and 4 post-inoculation. Mice were monitored daily for body weight change and survival for 14 days after challenge. Mice that had lost >25% of their initial body weight were humanely euthanized. Survival curves were estimated using the Kaplan Meier method and curves compared using the two-sided log rank test with subjects right censored, if they survived until the end of the study. *-$p < 0.05$; $p < 0.01$; ***-$p < 0.001$; ns – non-significant. Statistical analyses were performed using Prism v7.2 (GraphPad).

All infections were conducted under BSL-2^{+} containment and were authorized by the Institutional Ethics Committee on Experimental Animals at Icahn School of Medicine at Mount Sinai. For pulmonary titers, mice from each group (n = 3) were killed at 6 days (prophylaxis) or 5 days (therapy) post-inoculation and lungs were removed aseptically, snap frozen on dry ice and stored at −80°C until titration. Lungs were homogenized in 1 mL PBS using a Fastprep 24 homogenizer (MP Biomedicals). The homogenates were centrifuged (5 min, 16,100 x *g*, 4°C) to remove cellular debris and used for virus titration by plaque assay. Then, 200 μL of ten-fold dilutions of homogenized lungs in PBS were used for infecting confluent monolayers of MDCK cells. Virus was allowed to attach to MDCK cells for 1 h at 37°C. Cells were washed once with warm PBS and overlaid with oxoid agar (Oxoid, Basingstoke, Hampshire) prepared using $NaHCO_3$-buffered serum-free 2x MEM/BA containing DEAE Dextran and supplemented with TPCK-treated trypsin (1 μg/mL). Endpoint virus titers were determined by visualizing virus plaques 2 days after infection by staining with H1N1 post challenge serum (1/1,000 dilution), horseradish peroxidase-conjugated sheep-derived anti-mouse serum (GE Healthcare UK, NA-931) and TrueBlue substrate (KPL-Seracare, 5510-0031).

Prophylaxis Studies with Lethal Challenge and Therapeutic with Sublethal Challenge Mouse Model for Influenza A H1N1 Infection

For prophylaxis studies against lethal H1N1 challenge, groups of ten 6- to 8-month-old DBA/2J mice (The Jackson Laboratory) were treated with 10 mg/kg of either rFluA-20 IgG or positive control (CR6261) IgG or unrelated target control (MRSA-147) IgG 24-hours prior to being intra-nasally challenged with a lethal dose of 1,076 FFU of H1N1 A/California/07/2009. Mice were monitored for survival for 20 days after challenge. Moribund mice (little mobility), or mice that had lost >30% of their initial body weight (IACUC stipulated humane endpoint) were euthanized. Survival curves were estimated using the Kaplan Meier method and curves compared using the two-sided log rank test with subjects right censored, if they survived until the end of the study.

For therapeutic studies against sub-lethal H1N1 challenge, groups of ten BALB/c mice were challenged with a sublethal dose of 6.4×10^4 FFU and were given 10 mg/kg of FluA-20 IgG or CR6261 IgG or MRSA-147 IgG via the intraperitoneal route on day 1 post-inoculation. Mice were monitored for 14 days for weight change kinetics. Weight change curves were compared using 2-way Anova with Tukey's multiple comparisons test.

FluA-20 Prophylaxis Dose-Optimization against Mouse-Adapted Influenza A H1N1 Lethal Challenge

Experimental groups of 10 female BALB/c mice obtained from Charles River Laboratories (Wilmington, MA) were administered either 1, 3 or 10 mg/kg of FluA-20 IgG or 10 mg/kg of unrelated target control (mAb 2D22 specific for dengue virus envelope protein) IgG or 0.1 mL PBS by IP injection. At 24 h after mAb treatment, the mice were anesthetized by IP injection of ketamine/xylazine (50/5 mg/kg) followed by intranasal exposure to a 90 μL suspension of approximately 2,200 50% cell culture infectious dose ($CCID_{50}$)/mL) of mouse-adapted influenza H1N1 A/California/04/2009 virus that was kindly provided by Dr. Elena Govorkova (St. Jude Children's Research Hospital, Memphis, TN). Mice in a control group of 10 animals were treated with osteltamivir that was given by IP twice daily (bid) for 5 days, starting at 1 h post-infection. The animals were observed for 21 days and survival was based on body weight-loss cutoffs of <30% of initial weight. Survival curves were compared by the Mantel-Cox log-rank test. Mean day of death (MDD) comparisons were made by one-way ANOVA with Dunnett's multiple comparisons test. Differences in the number of survivors between mAb-treated and placebo groups were analyzed by the Fisher's exact (two-tailed) test. Calculations were made using Prism 8.0 (GraphPad Software, San Diego, CA). This study was conducted in the AAALAC-accredited laboratory animal research center of Utah State University in accordance with the approval of the institutional animal care and use committee of Utah State University.

Competition-Binding Groups

Biolayer interferometry on an Octet Red instrument (FortéBio) was used to perform competition-binding assays as described. Briefly, we loaded the HA from H1 A/California/04/2009 onto Ni-NTA tips at a concentration of 20 μg/mL, and then tested binding of two successively applied mAbs at 50 μg/mL. All antigen and Ab dilutions were made in 1X kinetic buffer (FortéBio, 18-5032). The Abs

were defined as competing Abs if the first Ab reduced binding of the second Ab by more than 70 percent. The Abs were defined as non-competing Abs if the first Ab reduced binding of the second Ab by less than 30 percent.

Fab and IgG Cloning, Expression, and Purification for Binding Kinetic Assay and X-Ray Crystal Structure Determination

FluA-20 Fab and IgG were expressed in 293F mammalian cells for determination of the binding kinetics and structures as previously described (Garces et al., 2015; Irimia et al., 2016). The heavy and light chains of the Fab were cloned independently into the phCMV3 vector and fused with the N-terminal IgK secretion signal peptide. A His_6 tag was added to the C terminus of the Fab heavy chain. Recombinant DNAs for both heavy and light chains were purified separately and co-transfected into 293F cells. The cells were cultured for 6 to 7 days at 37°C, while shaking at 125 rpm. Secreted Fabs were purified Ni-NTA Superflow (Qiagen), monoS chromatography (GE Healthcare).

To generate IgG for a given Ab, the DNA fragment of the V_H domain was fused with the DNA fragment of heavy chain Fc domain of human IgG1 via PCR. The full-length gene was cloned into the phCMV3 vector with the N-terminal IgK secretion signal peptide. IgG was expressed in 293F cells, as above, and purified by Protein G and monoS chromatography (GE Healthcare) and gel filtration.

Preparation of HA Head Domains

In brief, DNA fragments for the head domains (residues 52–263 of H1 HA [A/Solomon Islands/3/2006] and residues 43–306 of H3 HA [A/Hong Kong/1/1968]) were amplified separately with PCR reaction. The head domain DNA fragments were individually cloned into the pFastBac vector with an N-terminal gp67 secretion signal peptide and a C-terminal His_6 tag. Recombinant bacmid DNA was generated via the Bac-to-Bac system (Invitrogen) and baculoviruses were generated by transfecting purified bacmid DNA in to Sf9 cells. HA head domains were expressed by infecting the High Five cells with the recombinant virus, shaking at 110 rpm for 72 h at 28 oC. The secreted head domain protein was purified from the supernatant via Ni-NTA Superflow (Qiagen) and gel filtration on a Superdex75 column (GE Healthcare) in 20 mM Tris-HCl pH 8.0, 150 mM NaCl.

K_D Determination by Bio-Layer Interferometry

An Octet RED instrument (FortéBio) was used to determine K_D of the Ab-antigen interactions by bio-layer interferometry. The association and dissociation curves were processed using the Prism GraphPad. To examine the binding of FluA-20 or the UCA Fab to different HAs, biotinylated HA molecules were diluted to 10 to 50 μg/mL in PBS pH 7.4, 0.01% BSA and 0.002% Tween 20. HAs were immobilized onto streptavidin-coated biosensors (FortéBio) and incubated with FluA-20 or the UCA Fabs at highest concentration of 1 μM and with 2-fold dilution. The signals for each binding event were measured in real-time and K_d values determined by fitting to a 1:1 binding model.

Structure Determination of FluA-20 Fab and Complexes of FluA-20 with HA Head Domains

All complex samples were concentrated to 8 to 10 mg/mL for crystallization screening on our high-throughput robotic Rigaku CrystalMation system at TSRI using sitting-drop vapor diffusion. The conditions of crystals for x-ray data collection are as follows: Apo FluA-20 Fab (20°C; 0.2 M tri-sodium citrate, 20% (w/v) PEG3350, cryo-protected by addition of 15% glycerol); FluA-20_H1 head domain (20°C; 0.1 M phosphate-citrate, pH 4.2, 40% (v/v) PEG300; No additional cryo-protection); FluA-20_H3 head domain (4°C; 0.1 M Tris-HCl pH 8.5, 0.2 M lithium sulfate, 40% (v/v) PEG400; no additional cryo-protection). X-ray diffraction data were collected at multiple beamlines (Tables S3-4). The diffraction data were processed with HKL2000 and the structure was determined by molecular replacement in Phaser (McCoy et al., 2007). The initial models for FluA-20 were adapted from PDB 4KMT for the light chain and PDB 5BV7 for the heavy chain. The structures for H1 and H3 head domains were adapted from PDB models 4YJZ and 4FP8. Refinement was carried out in Refmac (Skubák et al., 2004), Phenix (Adams et al., 2010), model rebuilding was performed manually in Coot (Emsley and Cowtan, 2004), and the model was validated by MolProbity (Chen et al., 2010).

Structural Analysis

Interaction and interface analysis are carried out on online server PDBePISA at www.ebi.ac.uk/pdbe/pisa/. Structure figures were generated by MacPyMol (DeLano Scientific LLC).

Peptide Fragmentation and Deuterium Exchange Mass Spectrometry

To maximize peptide probe coverage, the optimized quench condition was determined prior to deuteration studies (Hsu et al., 2009; Li et al., 2011). In short, the HA head domain was diluted with buffer of 8.3 mM Tris, 150 mM NaCl, in H_2O, pH 7.15) at 0°C and then quenched with 0.8% formic acid (v/v) containing various concentration of GuHCl (0.8–6.4 M) and Tris(2-carboxyethyl) phosphine (TCEP) (0.1 or 1.0 M). After incubating on ice for 5 min, the quenched samples were diluted 4-fold with 0.8% formic acid (v/v) containing 16.6% (v/v) glycerol and then were frozen at −80°C until they were transferred to the cryogenic autosampler. Using the quench buffer of 6.4 M GuHCl, 1.0 M TCEP in 0.8% formic acid gave an optimal peptide coverage map.

The samples later were thawed automatically on ice and then immediately passed over an AL-20-pepsin column (16 μL bed volume, 30 mg/mL porcine pepsin (Sigma)). The resulting peptides were collected on a C18 trap and separated using a C18 reversed phase column (Vydac) running a linear gradient of 0.046% (v/v) trifluoroacetic acid, 6.4% (v/v) acetonitrile to 0.03% (v/v)

trifluoroacetic acid, 38.4% (v/v) acetonitrile over 30 min with column effluent directed into an Orbitrap Elite mass spectrometer (Thermo-Fisher Scientific). Data were acquired in both data-dependent MS:MS mode and MS1 profile mode. Proteome Discoverer software (Thermo Finnigan) was used to identify the sequence of the peptide ions. DXMS Explorer (Sierra Analytics, Modesto, CA) was used for the analysis of the mass spectra as described previously (Hamuro et al., 2004). FluA-20 mAb bound HAs were prepared by mixing FluA-20 mAb with monomeric H5 A/Vietnam/03/2204 HA head domain at a 1:1.1 stoichiometric ratio. The mixtures were incubated at 25°C for 30 min. All functionally deuterated samples, with the exception of the equilibrium-deuterated control, and buffers were pre-chilled on ice and prepared in the cold room.

Functional deuterium-hydrogen exchange reaction was initiated by diluting free HA or Ab-bound HA stock solution with D_2O buffer (8.3 mM Tris, 150 mM NaCl, in D_2O, pDREAD 7.15) at a 1:2 vol/vol ratio. At 10 sec, 100 sec and 1,000 sec, the quench solution was added to the respective samples, and then samples were frozen at −80°C. In addition, nondeuterated samples, equilibrium-deuterated back-exchange control samples were prepared as previously described (Hsu et al., 2009; Li et al., 2011; Lu et al., 2012). The centroids of the isotopic envelopes of nondeuterated, functionally deuterated, and fully deuterated peptides were measured using DXMS Explorer, and then converted to corresponding deuteration levels with corrections for back-exchange (Zhang and Smith, 1993).

Conservation Analysis of the FluA-20 Binding Epitope

Libraries for full-length and non-redundant human influenza H1 and H3 sequences were downloaded in January 2017 from the Influenza Virus Resource at the NCBI database (Bao et al., 2008). The H1 library includes 11,267 sequences and the H3 library includes 12,584 sequences. The HA sequence alignment was performed by MUSCLE (Edgar, 2004) and analyzed using EMBOSS program (Rice et al., 2000) and custom shell scripts based on SEQCONV+ (Roth Lab, UC Davis).

Conservation Analysis of the Overall HA Surface

A library of HA sequences that were recently isolated from human hosts since 2015 was used for surface conservation analysis, including 701 H1 sequences, 1,739 H3 sequences, and 17 other sequences of H5, H7 and H9 subtypes. The sequences were aligned with MUSCLE (Edgar, 2004) software and the conservation scores for each residue were analysis with ConSurf server (Ashkenazy et al., 2016; Celniker et al., 2013) and displayed on an H3 HA model (PDB 4O5N).

Comparison of FluA-20 Binding to HA0 and Cleaved HA Trimer by Biolayer Interferometry (BLI)

Baculovirus-expressed HA0 was prepared for the binding studies by cloning the HA ectodomain genes into the pFastBac vector with an N-terminal gp67 secretion signal peptide and a C-terminal BirA biotinylation site, thrombin cleavage site, foldon trimerization domain, and His_6 tag. HA0 was expressed in High five cells and the secreted HA0 purified from the supernatant via Ni-NTA Superflow (Qiagen) and gel filtration. The HA0 trimer fractions were concentrated for BLI assays. To prepare cleaved HA trimer, the HA0 trimer was incubated with trypsin at 4°C overnight (mass ratio of trypsin: HA0 ≈ 1:1,000). The HA cleavage was determined by SDS-PAGE electrophoresis with reducing agent. The cleaved HA was purified by gel filtration and the HA trimer concentrated for BLI assay. To evaluate Ab binding, Fabs of FluA-20 and RBS-Abs 5J8 for H1 binding (Hong et al., 2013) and H7.137 for H7 binding (Thornburg et al., 2016) were firstly immobilized onto anti-human CH1 biosensors (FortéBio) in the BLI buffer of PBS pH 7.4, 0.01% BSA and 0.002% Tween 20. The Fab-coated sensors were then incubated with corresponding HA0 and cleaved HA at 1 μM concentration for 120 s to evaluate the association, and then incubated with BLI buffer for 120 s to evaluate the dissociation.

Site-Directed Mutagenesis of Genes Encoding HA or Ab Proteins

Primers for site-directed mutagenesis were designed using the Agilent QuikChange Primer Design program (Agilent Technologies). The Quickchange Lightning Multi-Site Mutagenesis kit (Agilent, 210515-5) was used to introduce mutations into cDNAs encoding the Ab heavy chain genes or HA genes. The plasmids encoding mutants of FluA-20 heavy or light chains were transfected with the corresponding unmutated FluA-20 light or heavy chains, respectively. Abs encoded by cDNA with engineered mutations were purified and tested for binding to HA in ELISA, and the EC_{50} values for binding were determined using Prism software (GraphPad).

Influenza Viruses

The virus stocks were made from the supernatant of virus-infected MDCK cell culture monolayers in plain Dulbecco's Modified Eagle Medium (Gibco DMEM, Invitrogen, 11965) with 2 μg/mL of TPCK-trypsin. To obtain virus with uncleaved HA0 on the surface, the stocks were made by inoculating MDCK cells with virus for 1 hr. The cells were washed thoroughly and replenished with plain DMEM without TPCK-trypsin. The supernatant containing the virus was harvested at 48 h post inoculation.

Hemagglutinin Inhibition (HAI) and Microneutralization Assays

Neutralization potential of FluA-20 was determined by microneutralization and HAI assays, as previously described (Bangaru et al., 2016).

HA Cleavage Inhibition Assay

To assess the ability of FluA-20 to block HA cleavage, 4 μg of recombinant HA0 protein from H3 A/Perth/16/2009 was incubated with either PBS or 40 μg of mAb FluA-20 or mAb CR8020 for 1 h at 37°C. Following incubation, the Ab-HA mixture was either untreated or treated with 2.5 μg/mL of TPCK-treated trypsin and further incubated for 5, 20 and 40 min at 37°C. Samples were analyzed by SDS-PAGE.

pH-Dependent Conformational Change Assay

To determine the ability of FluA-20 to inhibit the low pH dependent conformational change in HA, 2.5 μg of pre-cleaved HA protein from H3 A/Perth/16/2009 was incubated with 5 μg of mAb FluA-20 or mAb CR8020. Reaction mixtures were incubated at 37°C for 1 h at pH 5.0. Separate reactions containing no Ab were incubated at pH 5.0 or pH 8.0 to be used as controls. Following incubation, all the mixtures were neutralized with pH 8.4 Tris buffer and were then either untreated or treated with TPCK-trypsin at 20:1 (WT:WT) ratio of HA to trypsin. Samples were incubated for 12 h at 37°C and then analyzed by non-reducing SDS-PAGE

Egress Assay

Cell culture monolayers of MDCK cells in 96-well plates were washed three times with PBS and inoculated with an MOI 1 of A/Texas/50/2012 H3N2 in Virus Growth Media with TPCK-treated trypsin (VGM) for 3 h at 37°C, 5% CO_2. The inoculum was removed from cells, and cells were washed three times with PBS. 10 μg/mL of mAbs in VGM: FluA-20, irrelevant control mAb MRSA-147 or known egress inhibitor IgG mAb H3v-47, or an equimolar concentration (66.7 nM) of the neuraminidase inhibitor drug zanamivir (GlaxoSmithKline) were added to cells in triplicate. Cells were incubated for 21 h at 37C, 5% CO_2. Supernatants were collected, clarified at 300 x *g* for 15 min to remove cell debris. Serial two-fold dilutions of supernatants in PBS were added to an equal volume of 0.5% turkey red blood cells in v-bottom plates to determine the virus titer by hemagglutination assay. Hemagglutination titers were determined as endpoint titer values.

Molecular Engineering of Ab Variable Gene Domains and Generation of Fc Mutants

For the expression of recombinant forms of Ab clones, nucleotide sequences of Ab variable domains were optimized for mammalian expression and synthesized on the BioXP 3200 System (SGI-DNA). These inserts were then joined with a 6.8-kb EcoR1/HindIII digested backbone of pML-huCG1 for expression of γ1 or BglII/NotI digested backbone of pML-huCk or pML-huCL vectors for κ or λ chains, respectively, using the NEBuilder HiFi DNA Assembly master mix (NEB, E2621). For the generation of Fc mutants, 4 nucleotide sequences of Ab constant domains with single mutations (K332A, D265A, and N297A) and a double mutant (L234A, L235A) in the constant heavy chain region (CH2) were optimized for mammalian expression and synthesized on the BioXP 3200 (SGI-DNA). These inserts were then joined with a 6.0-kb HindIII/XbaI digested backbone of pML-huCG1 (McLean et al., 2000) for construction of 4 separate γ1 mutant chains using the NEBuilder HiFi DNA Assembly master mix (NEB).

Dimeric Recombinant Soluble FcγRIIIa (CD16a) Binding ELISA

A dimeric recombinant soluble FcγRIIIa (rsFcγRIIIa) ELISA was used to model the need for ADCC-inducing Abs to cross link FcγRIIIa (Wines et al., 2016). A 96-well ELISA plate was coated with 50 ng of purified influenza HA protein from H1N1 A/California/07/2009 (Sino Biological, 11085-V08B) protein overnight at 4°C in PBS. The plates were treated as described (Wines et al., 2016). Briefly, the plates were blocked with PBS 1mM EDTA, 1% BSA (PBSE/BSA) for 1 h and 50 μL of Abs (FluA-20, FluA-45, FluA-55 or an unrelated negative control Ab [a recombinant form of HIV-specific mAb VRC01]) at various concentrations (40 μg/mL to 2.4 ng/mL) were added to the plates. The plates were washed with PBST (PBS with 0.1% Tween-20) and 50 μL of 0.1 μg/mL rsFcγRIIIa (V176) dimer was added to the wells and incubated for 1 h at 37°C. Pierce High Sensitivity Streptavidin-HRP (ThermoFisher Scientific, 21130) was diluted 1:10,000 in PBSE/BSA and added to wells. The plates were developed with TMB substrate solution and the reaction was stopped with 1 M HCl. The plates were read at an absorbance of 450 nm.

NK Cell Activation Assay

96-well ELISA plates were coated with 600 ng of purified influenza HA protein from H1N1 A/California/07/2009 (Sino Biological, 11085-V08B) overnight at 4°C in PBS. The plates were washed and incubated with 10 μg/mL, 1 μg/mL or 0.1 μg/mL of Abs (FluA-20, FluA-45, FluA-55 or VRC01) diluted in PBS for 2 h at 37°C. Plates were washed and 5 x 10^5 purified NK cells were added to each well. NK cells were purified from freshly isolated PBMCs using the EasySep human NK cell enrichment kit (STEMCELL Technologies, 19055). Mouse anti-human CD107a allophycocyanin-H7 Ab (clone H4A3; BD Biosciences, 561343), 5 μg/mL brefeldin A (Sigma-Aldrich, B6542) and 5 μg/mL monensin (BD GolgiStop; BD Biosciences, 554724) were added to the cells and incubated for 5 h. Purified NK cells then were incubated with anti-human CD3 PerCP (clone SP34-2; BD Biosciences, 552851) and anti-human CD56 allophycocyanin (clone B159; BD Biosciences, 555518) for 30 min at RT. Cells were fixed and permeabilized for 10 min and then incubated with anti-human IFNγ AF700 (clone B27; BD Biosciences, 561024) in the dark. Finally, cells again were fixed with 1% formaldehyde, and data were acquired for 20,000 – 50,000 events using an LSRFortessa flow cytometer (BD Biosciences).

In Vivo Efficacy of FluA-20 Fc Mutants

To determine the contribution of FluA-20 Fc-mediated activity to overall protection observed *in vivo*, groups of BALB/cJ mice were prophylactically treated with 10 mg/kg of either FluA-20 IgG1 or rFluA-20 IgG1 or rFluA-20-N297A IgG1 or rFluA-20-LALA IgG1 or MRSA-147 IgG 24-hours prior to being intra-nasally challenged with 1.2 x 10^4 focus forming units (FFU) of H1N1 A/California/07/2009. Mice were monitored for 14 days for weight change and disease (clinical score).

Sublethal Respiratory Challenge Mouse Model for Influenza A H1N1 Infection

Groups of BALB/c mice were inoculated intranasally with different doses (538, 2,690, 13,400, or 67,000 FFU) of A/California/04/2009 virus and were monitored for 14 days for weight change kinetics and the disease. Weight loss of more than 20% total weight was the IACUC stipulated endpoint for humane euthanasia. Based on the results obtained from this study, a dose of 1.2 x 10^4 FFU was deemed appropriate for the challenge studies with FluA-20 Fc mutants.

Focus Size Reduction Assay

To examine the ability of mAb FluA-20 to reduce focus size, a predetermined amount of H3N2 A/Hong Kong/1/1968 virus was incubated with dilutions (10, 5, or 1 μg/mL) of mAb FluA-20 or irrelevant control mAb MRSA-147 or mAb CR9114 or molar equivalents of zanamivir in the presence of TPCK-treated trypsin for 1 h at 37°C. The mixture then was used to inoculate a monolayer of MDCK cells in 6-well plates, followed by incubation at 37°C for 1 h with intermittent rocking. The Avicel overlay (1.2% Avicel in DMEM) supplemented with the corresponding mAb dilutions and 1 μg/mL of TPCK-treated trypsin then was added to each well. The plates were incubated for 48 h at 37°C. Following incubation, the plates were washed and fixed with 1 mL of 80% methanol/ 20% PBS. The presence of influenza nucleoprotein in the fixed cells was determined using a 1:6,000 dilution of mouse anti-NP Ab (BEI Resources, NR 4282) as the primary Ab and 1:500 of peroxidase-labeled goat anti-mouse Abs (SeraCare) as the secondary Ab. The foci were visualized subsequently using TrueBlue peroxidase substrate (KPL). Images were captured by an CTL Immunospot S5 Analyzer. Foci area as percentage of total area was calculated by ImageJ software (NIH).

Flow Cytometric Analysis of Ab Binding to Cell-Surface-Expressed HA

HEK293F cells grown in expression medium (Freestyle 293 Expression Medium; Invitrogen, 12338) were transfected transiently with cDNA encoding H3 A/Hong Kong/1/1968 HA protein and incubated at 37°C for 36 h. Untransfected (UT) or transfected cells were washed and treated with either DMEM containing TPCK trypsin (2 μg/mL) or plain DMEM for 15 min at 37°C. Cells were washed with PBS containing 2% of heat inactivated FBS and 2 mM EDTA (FACS buffer) and incubated with either mAb CR9114 or mAb FluA-20 (10 μg/mL) for 30 min at RT and for 5 min at 37°C. The cells were washed with FACS buffer and incubated with secondary goat anti-human IgG PE Ab (Southern Biotech, 2040-09) for 1 h at 4°C, fixed with 4% formaldehyde in PBS, and analyzed by flow cytometry using an LSR-2 cytometer (BD Biosciences). Data for a total of up to 20,000 of cell events were acquired and analyzed with FlowJo software (Tree Star).

HDX-MS to Comparison the Dynamic Change of H7 HA0 Trimer and Cleaved HA Trimer

H7 HA (A/Netherlands/219/2003) was expressed in HEK293F cells (Bangaru et al., 2016). In brief, sequences encoding the HA genes were optimized for expression, and cDNAs were synthesized (Genscript) as soluble trimeric constructs by replacing the transmembrane and cytoplasmic domain sequences with cDNAs encoding the GCN4 trimerization domain and a His-tag at the C terminus. Synthesized genes were subcloned into the pcDNA3.1(+) mammalian expression vector (Invitrogen). HA protein was expressed by transient transfection of 293F cells with polyethylenimine transfection reagent and grown in expression medium (Freestyle 293 Expression Medium; Invitrogen, 12338). The HA0 protein was harvested after 7 days with HisTrap TALON FF crude columns and the HA0 trimer purified via gel filtration. To obtained cleaved HA trimer, the HA0 protein was treated with trypsin at 37°C for 30 mins and the cleaved HA trimer further purified by gel filtration.

Prior to conducting comparative hydrogen-deuterium exchange experiments with H7 HA0 or with cleaved H7HA, the quench condition for best sequence coverage of HA was 6.4 M GuHCl, 1 M TCEP and 0.8% formic acid, as previously described (Aiyegbo et al., 2014; Li et al., 2011; Marsh et al., 2013). To initiate hydrogen-deuterium exchange reactions, 2 μL of pre-chilled protein stock solution (free un-cleaved H7 HA0, 1.8 mg/mL; cleaved H7 HA, 1.6 mg/mL) was diluted into 4 μL D_2O buffer (8.3 mM Tris, 150 mM NaCl, in D_2O, pDREAD 7.2) at 0°C. At indicated times of 10 sec, 100 sec, 1,000 sec, 10,000 sec and 100,000 sec, the exchange reaction was quenched by the addition of 9 μL of optimized quench solution at 0°C. After incubating on ice for 5 min, the quenched sample was diluted 5- fold with 0.8% formic acid containing 16.6% glycerol, immediately frozen on dry ice and stored at −80°C. In addition, un-deuterated samples and equilibrium-deuterated control samples were also prepared. All samples were then loaded onto our in-house LC instrument for online digestion and separation (Aiyegbo et al., 2014). The resulting peptides were directed into an OrbiTrap Elite Mass Spectrometer (Thermo Fisher Scientific, San Jose, CA) for DXMS analysis. Instrument settings have been optimized for HDX analysis. The data acquisition was carried out in a data-dependent mode and the five or ten most abundant ions were selected for MS/MS analysis. Proteome Discoverer software was used for peptide identification. The centroids of each peptide was calculated with HDExaminer, and then converted to corresponding deuteration levels with corrections for back-exchange (Zhang and Smith, 1993).

Negative Stain Electron Microscopy

FluA-20 Fab was incubated with uncleaved H1 HA trimer for 20 seconds at 5 times molar excess of Fab. The complex was added to carbon-coated 400 mesh cooper grids and stained with 2% uranyl formate. Micrographs were collected on a 120kv Tecnai Spirit microscope with a 4kx4k TemCam F416 camera using Leginon (Potter et al., 1999). Images then were processed with Appion (Lander et al., 2009). Particles were selected with DoGpicker (Voss et al., 2009), and 2D classes were generated with MSA/MRA (Ogura et al., 2003). Particles were false colored in Photoshop.

DATA AND SOFTWARE AVAILABILITY

The accession numbers for the atomic coordinates and structure factors are Protein Data Bank (PDB): 6OBZ, 6OC3, and 6OCB.

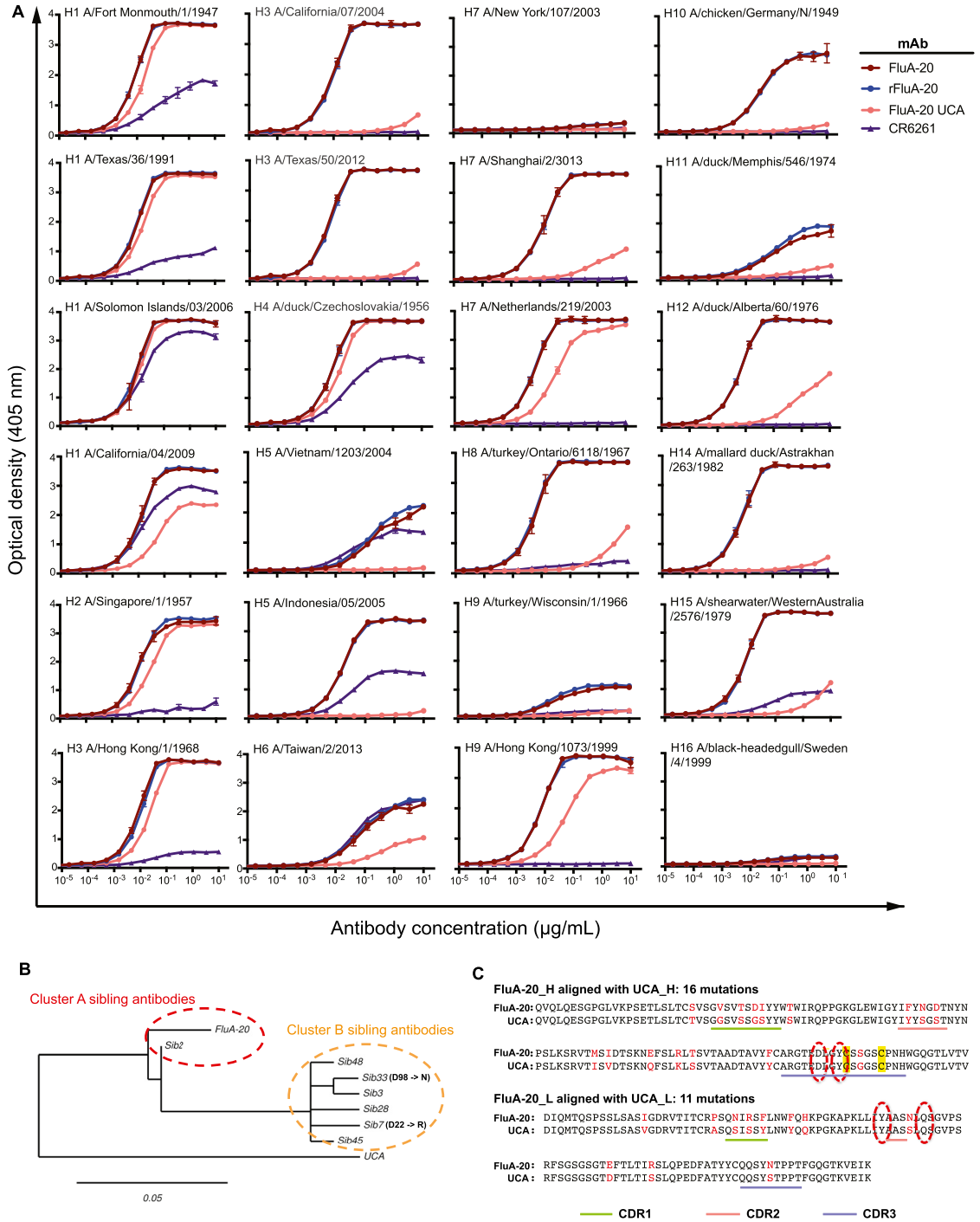

Figure S1. Binding of FluA-20 Ab to HA, Related to Figure 1 and Table S1

(A) Binding curves for mAbs FluA-20, rFluA-20, or FluA-20-UCA or an irrelevant control IgG (anti-MRSA) against HAs derived from indicated strain and subtype, as determined by Enzyme Linked Immunosorbent Assay (ELISA).

(B) Phylogenetic tree of representative sibling Abs of FluA-20 that were tested for binding.

(C) Amino acid sequence of FluA-20 and the unmutated common ancestor (UCA) of FluA-20 are aligned. Mutated residues are colored as red and a unique disulfide bond in CDR H3 is highlighted in yellow. The key residues Asp98 (H), Tyr100a (H), Tyr48 (L), and Gln55 (L) that were later identified as critical for the interaction with HA are present in the UCA sequence (indicated by red dashed circles).

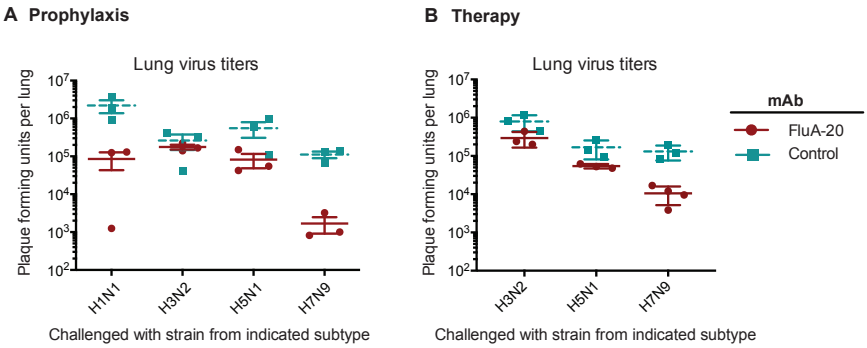

Figure S2. Lung Titers of Mice Treated with FluA-20 in Prophylactic or Therapeutic Settings, Related to Figure 2

(A) Groups of mice (n = 3) were treated prophylactically with 10 mg/mL of either FluA-20 or a similarly prepared control Ab to an unrelated target (MRSA) and challenged 24 h later with a sublethal dose of 0.1 LD_{50} with either H1N1 A/Netherlands/602/2009 or H3N2 A/X-31 (6:2 PR8 backbone) or H5N1 A/barn swallow/Hong Kong/D10-1161/2010 (7:1 PR8 backbone) or H7N9 A/Shanghai/1/2013 (6:2 PR8 backbone). Lung samples were collected from mice for each Ab treated group at 6 days post-inoculation. The graph shows pulmonary virus titers in FluA-20 and control treated mice.

(B) Groups of mice (n = 3) were lethally challenged with 1.2 LD_{50} of H3N2 A/X-31 or H5N1 A/barn swallow/Hong Kong/D10-1161/2010 or H7N9 A/Shanghai/1/2013 on PR8 backbone and were treated therapeutically with 10 mg/kg of FluA-20 or an irrelevant Ab (MRSA) via the intraperitoneal route on days 1, 2 and 4 post-challenge. Lungs were collected for virus titration at 5 days post-inoculation.

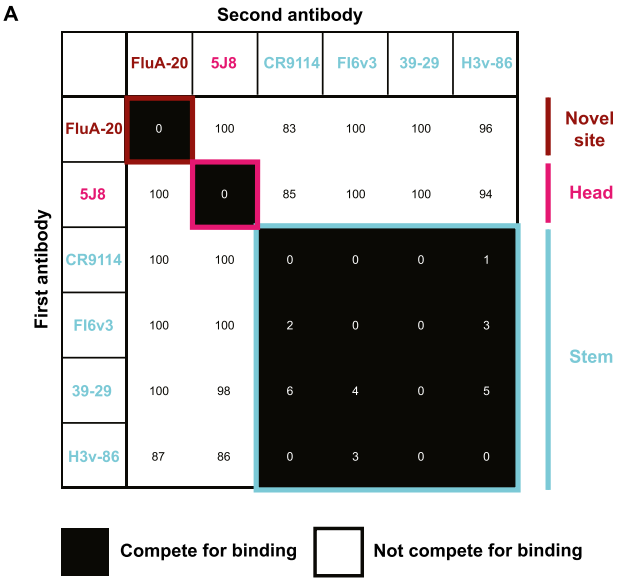

Figure S3. Binding of FluA-20 Ab to a Unique Site on the HA Head Domain, Related to Figure 3

(A) Competition-binding assays were performed using bio-layer interferometry. The His-tagged A/California/07/2009 H1 HA was loaded onto Ni-NTA tips, and binding of two successively applied Abs (IgG) was tested. MAb FluA-20 was competed against mAb 5J8, a receptor binding site mAb, or each of four stem-binding Abs: CR9114, FI6v3, 39.29 or H3v-86. FluA-20 did not compete with either the RBS- or the stem-specific Abs indicated.

(B) FluA-20 IgG was immobilized on anti-human Fab CH1 biosensors. Strong binding to the head domains (0.5 μM concentration) of H1 (A/Solomon Islands/3/2006), H3 (A/Victoria/361/2011) and H7 (A/Shanghai/02/2013) HAs was observed for immobilized FluA-20 in a BLI assay.

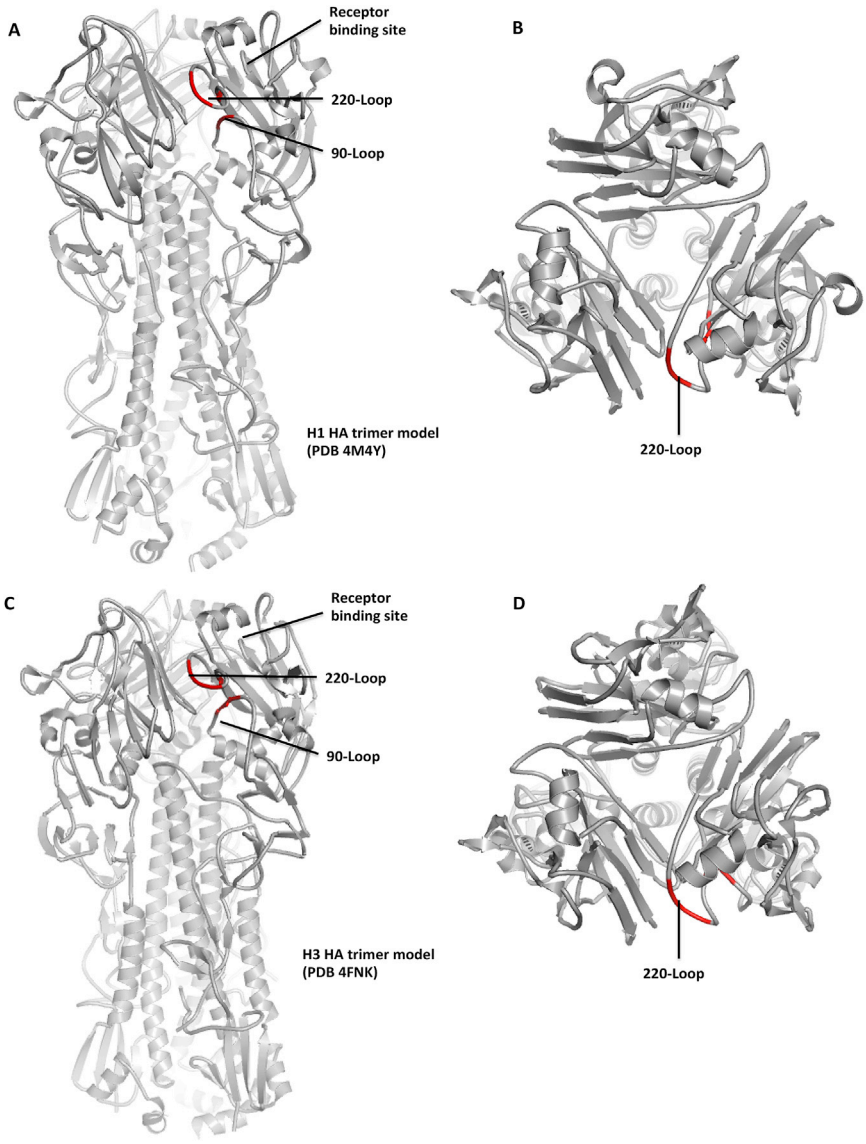

Figure S4. FluA-20 Binds to the 220-Loop and 90-Loop of H1 and H3 HA, Related to Figures 3 and 4

(A and B) H1 HA trimer of A/California/04/2009 is shown in a secondary structure representation. Residues identified to be in the H1 epitope (Pro96, Ile219, Arg220, Pro221, Lys222, Val223, and Arg229) that are contacted by FluA-20 are colored in red. These residues interact with the adjacent protomer in the unliganded HA trimer crystal structure.

(C and D) H3 HA trimer of A/Hong Kong/1/1968 is shown in a secondary structure representation. The key interacting residues in the H3 epitope (Pro96, Ser219, Arg220, Pro221, Trp222, Val223, and Arg229) that are contacted by FluA-20 are colored in red. Many of these residues interact with the adjacent protomer in the unliganded HA trimer crystal structure.

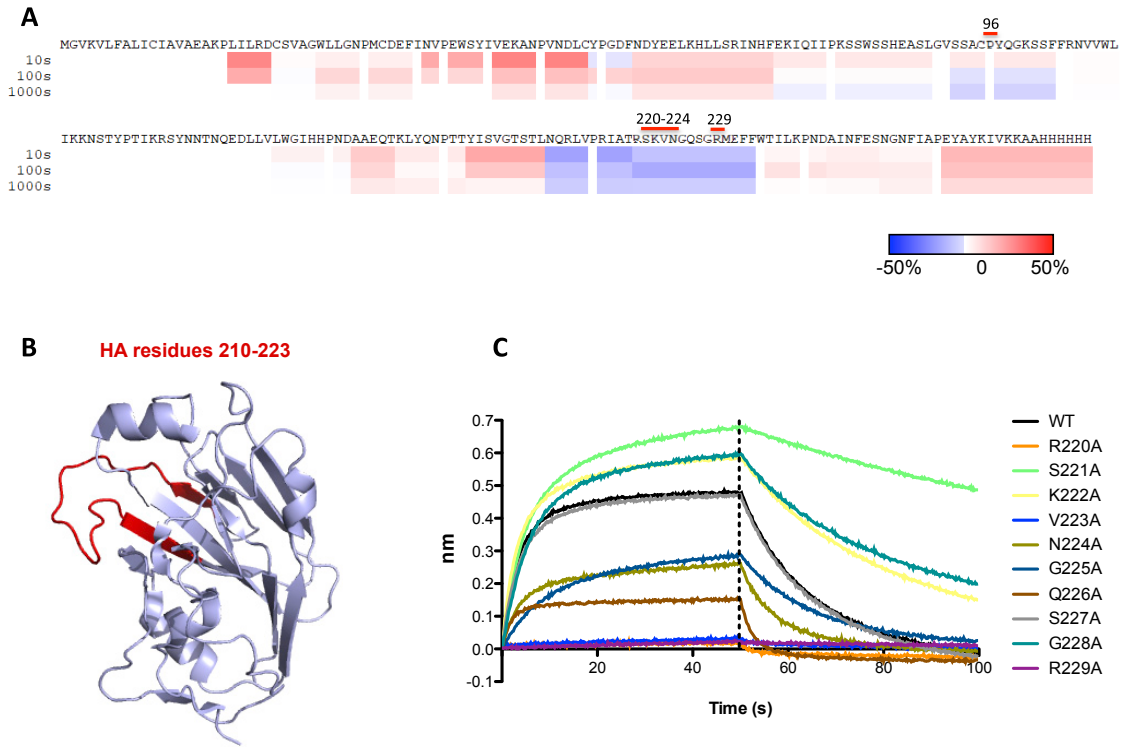

Figure S5. H5 Epitope Mapping with FluA-20 by HDX-MS and Mutagenesis, Related to Figure 5

(A) Difference map from deuterium exchange of the H5 head domain from A/Vietnam/1203/2004 (H5N1) with or without FluA-20 binding. Residues with slower deuterium exchange in the presence of FluA-20 are colored in blue and residues with faster exchange are colored in red; white regions indicate peptides for which there was no coverage.

(B) Regions of HA with slower deuterium exchange after binding FluA-20 are mapped in red onto the surface of H5 VN/1203 head domain (purple).

(C) Mutations of the 220-loop residues substantially influence binding of FluA-20 IgG (as measured by BLI assays, using 25 μg of IgG). The R220A, V223A, or R229A mutations in H5 HA completely eliminated FluA-20 binding, whereas N224A, G225A, or Q226A mutants decreased FluA-20 binding. Mutations S221A, K222A, and G228A each appeared to enhance FluA-20 binding slightly.

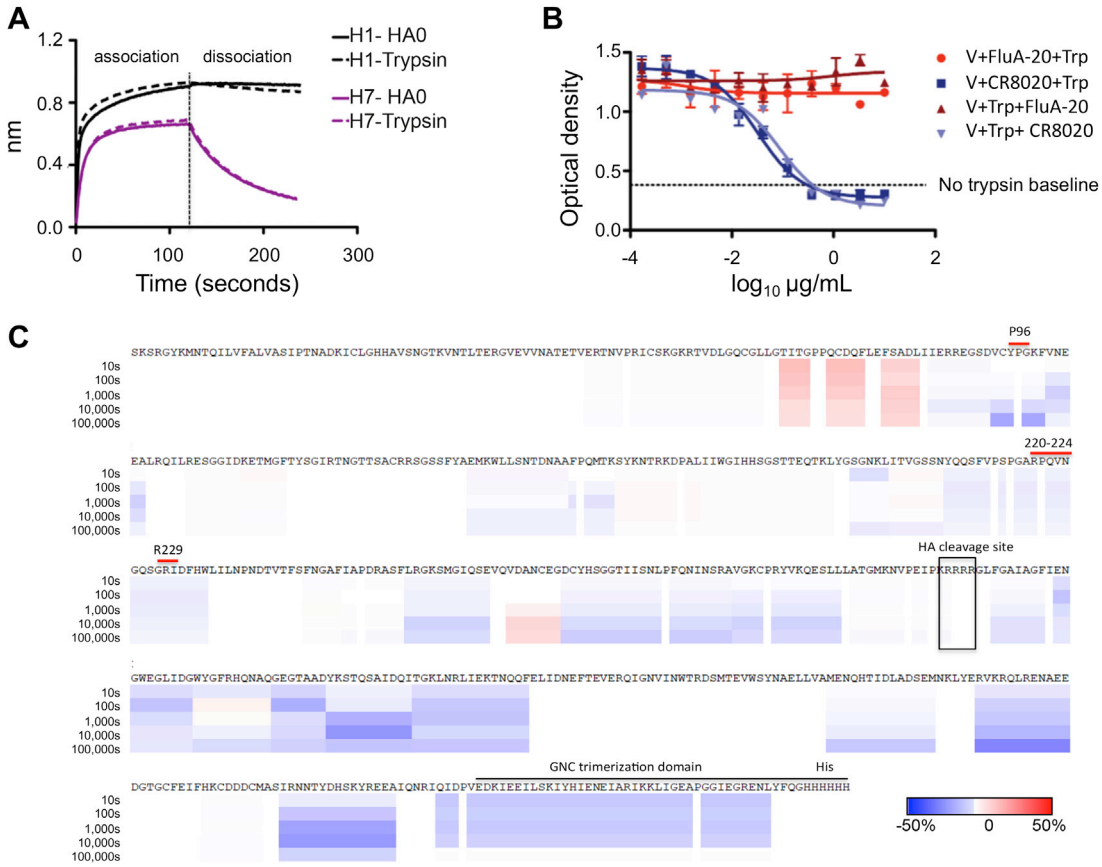

Figure S6. Comparison of Ab Binding to HA0 versus Cleaved HA Trimers, Related to Figure 6

(A) Binding traces of HA0 trimer or cleaved HA trimer (HA1/HA2) to receptor-binding site Abs. The Ab used for binding to H1 HA (A/California/04/2009) was 5J8 and for H7 HA (A/Shanghai/02/2013) was H7.137.

(B) HA0 [from A/Hong Kong/1/1968 (H3N2)] virus (V) produced in the absence of trypsin was incubated with serial dilutions of mAbs (FluA-20 or CR8020) either before or after treatment with 1 µg/mL of trypsin (Trp) at 37°C for 45 min. The samples were trypsin-inactivated with 10% FBS before adding to MDCK cell monolayers. As a control, HA0 virus untreated with trypsin (and therefore inactive) was also added to MDCK cell monolayers. Following incubation, the cells were fixed and the presence of influenza nucleoprotein in the cells was determined by ELISA using a mouse anti-NP Ab. The dotted line indicates the baseline signal from the noninfectious HA0 virus (untreated).

(C) Difference map from deuterium exchange of cleaved HA trimer compared to HA0 trimer from A/Netherlands/219/2003(H7N7) by HDX-MS.

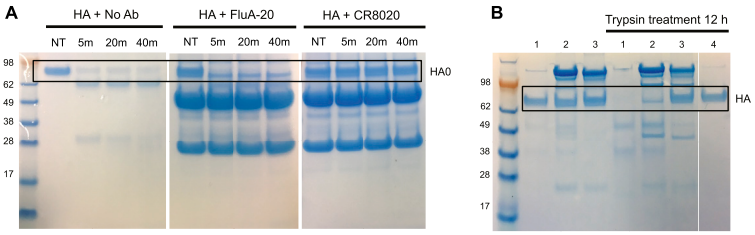

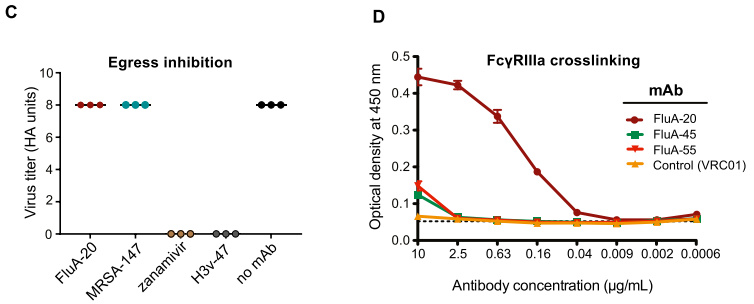

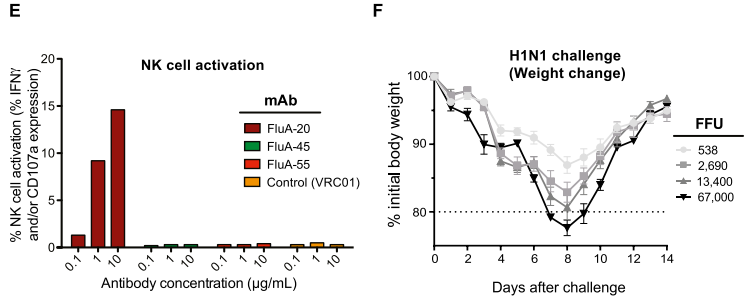

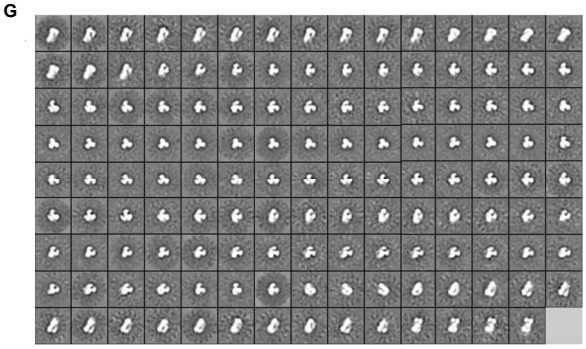

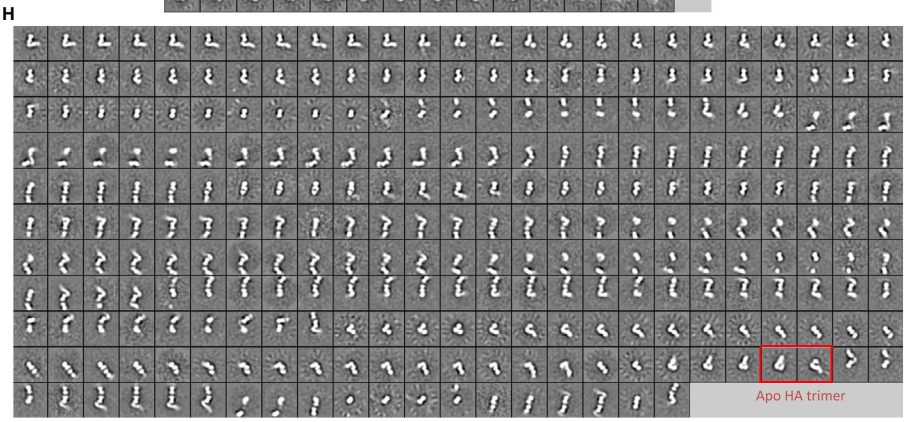

(legend on next page)

Figure S7. Functional Characterization of FluA-20 IgG, Related to Figure 7

FluA-20 was tested for (A) HA cleavage inhibition, (B) pH-induced HA conformational change inhibition, and (C) egress inhibition.

(A) SDS-PAGE of 4 μg of recombinant HA0 protein (from A/Perth/16/2009 (H3N2) that was premixed with either PBS or 40 μg of mAb FluA-20 or mAb CR8020 was either not treated (NT) or treated with TPCK-trypsin for 5, 20, or 40 min at 37°C.

(B) Non-reducing SDS-PAGE of recombinant HA (H3 Perth) pre-incubated with either (1) PBS, (2) mAb FluA-20, or (3) mAb CR8020 for 1 h at pH 5.0 were neutralized to pH 8.4 and further treated with PBS or TPCK-trypsin for 12 h. HA was also incubated with (4) PBS at pH 8.0 and treated with trypsin at pH 8.4 as a control.

(C) Egress inhibition of FluA-20 was tested using H3 Texas virus. Hemagglutination titer value was used to confirm virus egress from cell surface to supernatant. Data represent one of two independent experiments, each dot represents value per repeat, and lines represent the mean and standard deviation of assay triplicate.

(D) Cross-linking of FcγRIIIa. Binding curves were obtained by performing ELISA with serial dilutions of each Ab (FluA-20 and control mAbs FluA-45 or FluA-55 or HIV-specific mAb VRC01) onto HA-coated plates and assessing the ability of HA-bound mAbs to engage both Fc-binding sites on the soluble FcγRIIIa dimer. The dotted line indicates the limit of detection.

(E) FluA-20 or control mAbs were each added independently on 96-well plates coated with purified A/California/07/2009 H1 HA. The percentage of NK cell activation was calculated from the number of NK cells incubated with HA-bound Ab that expressed CD107a and/or IFNγ.

(F) Sub-lethal respiratory challenge mouse model for influenza A H1N1 infection. Groups of BALB/c mice were inoculated i.n. with indicated dose of A/California/04/2009 virus and monitored for 14 days for weight change kinetics. Data represent the mean value ± SEM, using five mice per group. The dotted line indicates the endpoint for humane euthanasia.

(G) Images of H1 HA0 trimer (A/California/04/2009) show intact trimer conformation without exposure of FluA-20 Fab.

(H) 2D class average of H1 (A/California/04/2009) HA bound by FluA-20 Fab after 20-second incubation; only the monomeric form of the complex was observed. A few apo HA trimers also were observed, as denoted by the red box.